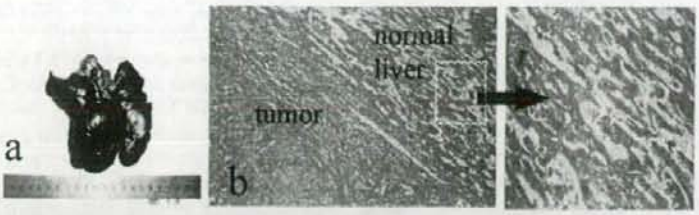

Fig. 4. Photographs (a) and sections of rabbit VX2 tumor with Perls staining (b) after MR imaging enhanced with SPIO-alginate. Iron oxide particles were not found in the tumor part, but in the normal part of the liver (magnification ×10).

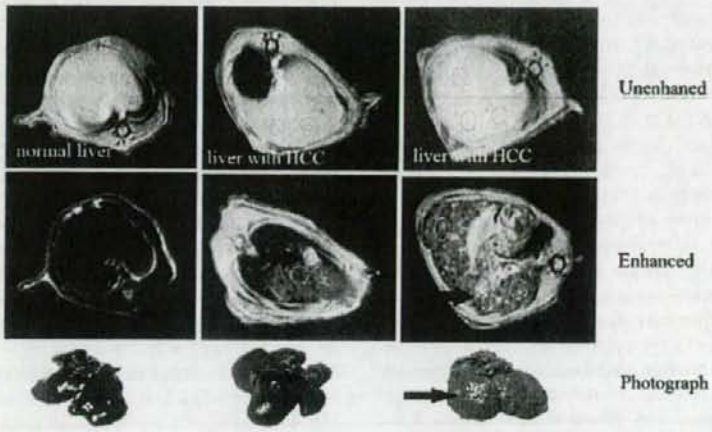

Fig. 5. T2*-weighted GRE images and photographs of liver with primary cancer in rats. No HCC was found on unenhanced images, however, some HCC were found (arrow) on SPIO-alginate enhanced images. The center photograph showed the liver of model rat has one HCC and slight cirrhosis, and the right-hand side photograph showed the liver of model rat has more HCC and severe cirrhosis.

mal rat on enhanced images decreased significantly, slightly decreased for cirrhosis, and almost did not decrease for HCC. Furthermore, there were hyperplastic nodules and some hemorrhage in photographs of model rats' liver. Fig. 6 showed the sections of liver with Perls staining after MR imaging scan, ranging from 2 to 12 h after injection of 20 μmol Fe/kg of SPIO-alginate, which indicated that iron oxide particles were present in normal liver, hyperplastic nodule and hemangioma, rather

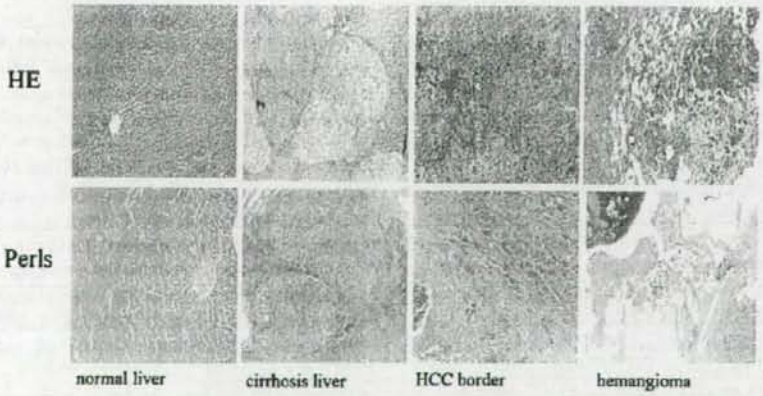

Fig. 6. Light micrograph with HE staining and Perls staining of liver in rats with primary cancer after MR imaging scan within 2–12 h after injection of 20 μmol Fe/kg of SPIO-alginate. According to HE staining, the liver structure of control group was normal, and that of tumor model group accompanied with cirrhosis. Besides HCC, hyperplastic nodule, and hemangioma were identified. As for Perls staining, iron oxide particles were detected in the hemangioma and hyperplastic nodule, rather than in HCC (magnification ×10).

than in HCC. All the livers of model rats were accompanied by cirrohsis according to HE staining. Meanwhile, some HCCs, hyperplastic nodules, and hemangiomas were indentified.

4. Discussion

The alginate used in the study is of pharmaceutical grade which has been approved for oral administration as an inactive ingredient in human. Moreover, sodium alginate was studied for intravenous injection in some animals, and the LD_{50} was described as less than 200 mg/kg for mouse, approximately 100 mg/kg for rabbit (Solandt, 1941), and 1000 mg/kg for rat (Sokov, 1970). In this study, the amounts of sodium alginate used in rats were about 40 mg/kg, which is far less than the LD_{50} (Sokov, 1970). Furthermore, alginate is considered biocompatible and biodegradable in tissues. Alginate has been reported to undergo proton catalyzed hydrolysis which is dependent on time, pH, and temperature (Gombotz and Wee, 1998; Bouhadir et al., 2001; Robitaille et al., 1999). In addition, the chemical composition and the mitogenic contaminants found in alginate are the two main contributors to alginate immunogenicity including cytokine release and inflammatory reactions (Gombotz and Wee, 1998). Hence, the degradatioin of alginate in SPIO-alginate might result in the edema of hepatocytes.

Pharmacokinetics and tissue distribution of SPIO-alginate after intravenous injection were quantitatively studied by determining the iron concentration in blood, serum and tissues. Although it was difficult to differentiate between the endogenous iron and the injected iron, it was reliable to reflect the *in vivo* behavior of SPIO-alginate by subtracting the endogenous iron concentration and this method was used in some studies (Taupitz et al., 2004; Bourrinet et al., 2006). The phenomenon that the blood iron concentration values were under the initial concentration before injection (about 471.9 μg/mL) was observed from about 6 to 48 h after administration of SPIO-alginate, alginate solution and saline, was speculated these might be caused by the several bleedings. After several bleedings, red blood cell count would decrease and therefore there would be a decrease in iron content in blood samples. The blood iron concentration began to increase to initial level at 96 h after injection for both SPIO-alginate, which might be resulted from the fact that SPIO-alginate after uptake by macrophages was degraded by the lysosomes, and then the iron entered the plasma iron pool and was subsequently incorporated into red cell production (Pouliquen et al., 1991; Weissleder et al., 1989).

Since blood loss could significantly decrease red blood count and blood iron concentration, it was better to evaluate the pharmacokinetics of SPIO-alginate in serum, even though the basic serum iron concentration fluctuated according to different rats. In our study, the serum iron concentrations at various time points after injection of alginate solution were in the range of basic serum iron concentration (Table 1). Hence, it indicated that the intravenous injection of alginate solution had no effect on serum iron concentration. We speculated that the COO^- terminals of alginate might not bind the iron in serum. On the other hand, the half-life of SPIO-alginate in serum were 0.27 ± 0.05 h at 109.5 μmol Fe/kg and 0.65 ± 0.22 h at 218.9 μmol Fe/kg in rats in Table 2. C_{max}, $T_{1/2}$, AUC and MRT in serum with the high dose were significantly higher than those of the low dose ($P < 0.05$). After intravenous injection, SPIO-alginate accumulated dominantly in the liver and spleen with a total percentage of more than 90% (Table 3).

As an MR contrast agent, the physicochemical properties including the size of the particle, the charge and the nature of the coating, and the dose will determine the stability, distribution and metabolism of SPIO agents, and then will certainly affect MR imaging (Gupta and Gupta, 2005; Wang et al., 2001; Neuberger et al., 2005). According to the previous studies, the particle size played a very important role. The larger the particles, the shorter the plasma half-life is (Wang et al., 2001). Since SPIO uptake into the RES is related to protein absorption on the particle surface and subsequent opsonization, minimizing the particle size will ultimately reduce particle phagocytosis, finally resulting in a significant increase in plasma half-life and wider biodistribution (Neuberger et al., 2005). Although SPIO-alginate used in this research had a mean core diameter of about 5–10 nm, the big hydrodynamic diameter of 193.8 nm and high negative ξ-potential might explain the fast clearance from blood and the accumulation mostly in the liver and spleen (Table 2). This result was in accordance with the report that the blood half-life of Ferumoxides was 6 min and efficiently accumulated in the liver (approximately 80% of the injected dose) and spleen (5–10% of the injected dose) with minutes of administration (Wang et al., 2001). The amount of iron oxide (about 10–20 μmol Fe/kg body weight) for clinical MR imaging is small compared with other MR contrast agents and extensive toxicity studies in animals have indicated no acute or chronic toxicity at doses greater than 100 times the clinical effective dose (Weissleder et al., 1989; Reimer et al., 1995).

For specific characterization of liver lesions, the tissue-specific contrast agent should be located predominantly in one tissue. The distribution of contrast agent in liver is rather complicated, as it can be located in the extracellular space including blood and interstitium, and cellular space including reticuloendothelial cells, hepatocytes and endothelial cells. In our study, Perls staining did not show iron within hepatocytes but mainly within the KCs. Furthermore, the account of SPIO-alginate in the liver peaked at 0.5 h with the dose of 109.5 μmol Fe/kg from quantitative iron concentration (Table 3) and qualitative histology evaluation (Fig. 1). This suggested that SPIO-alginate could not act as an extracelluar agent during the early time points. These results were in accordance with the liver enhancement of SPIO-alginate in normal rat, in which a significant decrease of the liver signal intensity on T1-weighted images at 10 min was observed (Fig. 2). It was reported that positive enhancement on T1-weighted images was observed when the iron particles were extracelluar. When the particles were intracellular, only a negative enhancement was seen (Oswald et al., 1997; Van Beers et al., 2001). It was suggested that the uptake of contrast agents of negative ξ-potential was mediated by scavenger receptors expressed in both Kupffer and liver endothelial cells (Seternes et al., 2001). Compared to KCs, liver endothelial cells were believed to be less effective at metabolizing and degrading particulate iron (Briley-Sæbø et al., 2004). The half life of SPIO-alginate in

liver at a dose of 109.5 μmol Fe/kg was about 139.1 h (Table 2) and only small iron was observed at 336 h after injection from Perls staining (Fig. 1). Hence, we speculated that there was little or almost no SPIO-alginate in endothelial cell. In sum, the distribution of SPIO-alginate in liver was predominately in KCs, which was just the mechanism of SPIO-alginate to detect liver tumors.

A negative enhancement of the liver was observed on both T1- and T2-weighted images after injection of SPIO-alginate in normal rats (Fig. 2). Compared with the corresponding unenhanced images, SNR on enhanced images decreased by 2.32 times with T1-weighted FSE sequence, 8.02 times with T1-weighted SPGR sequences, 3.88 times with T2-weighted IRFSE sequence, and 8.64 times with T2*-weighted GRE sequence. The negative enhancement on T1-weighted images might be caused by the physical characteristics of the individual nanoparticles. In other words, the high-field magnetization of the iron oxide core could be sufficient to relax water protons effectively, which might attribute to the fact that iron oxide was not simply coated by alginate polymer (Ma et al., 2007). Furthermore, the results also indicated that SPIO-alginate did not agglomerate *in vivo* (Kellar et al., 2002). Meanwhile, the intracellular iron particles mentioned above might be another reason for the negative enhancement on T1-weighted images. On the other hand, the negative enhancement effect of SPIO-alginate on T2- and T2*-weighted images was demonstrated, and GRE images were more sensitive to susceptibility effects than FSE images according to earlier report (Ward et al., 2003).

SPIO-alginate was mainly phagocytosed by liver after intravenous administration as mentioned above. As a result, these particles taken up in liver could accelerate T2 relaxation by creating local inhomogeneities in the magnetic field, causing reduced signal intensity on both T1- and T2-weighted images, but most remarkable decrease on acquisitions with T2*-weighted. In this study, HCC was not found at pre-SPIO on T2*-weighted images, but found at post-SPIO, for the signal intensity of HCC was significantly higher than that of the adjacent liver parenchyma (Fig. 5). Hence, MR imaging with SPIO-alginate enhancement was shown to improve the detection of HCC in the cirrhotic liver compared with unenhanced imaging. Our study confirmed these expectations, as did most published studies of the recent years (Saini et al., 1987; Clement et al., 1991; Nakayama et al., 1998; Imai et al., 2000; Bourrinet et al., 2006).

The efficacy of iron oxide to enhance the transverse relaxation rates ($1/T2^* = R2^*$) in the liver depended upon its initial distribution or uptake into the liver. Factors which may alter the uptake of SPIO particles and the resultant effect on signal intensity include phagocytic activity, clustering of the particles, and local blood flow.

First of all, the change of signal intensity in liver on SPIO enhanced MR imaging is mainly mediated by phagocytic activity. And phagocytic activity is depended on both the number of sinusoidal KCs per unit volume of liver parenchyma (KCs tissue density) and individual KCs function. It is suggested that the number of KCs in dysplastic nodules or in cirrhosis is similar to that in adjacent liver parenchyma, and the number of KCs in HCC decreased as the tumors became less well differentiated (Imai et al., 2000). It has been reported that SPIO-enhanced MR imaging can evaluate the number and function of KCs (Tanimoto et al., 2002). In our studies, iron oxide particles were found in normal liver and hyperplastic nodule, rather than in HCC and VX2 tumor from histological evaluation (Figs. 4 and 6).

It has been reported that the signal intensity changes induced by SPIO may vary according to the spatial distribution of particles and cluster size on relaxation times within KCs in T2*-weighted sequences and T2*-insensitive weighted sequences (Imai et al., 2000). Additionally, large intracellular SPIO clusters produced greater SNR loss on GRE images than small clusters because of the magnetic susceptibility effects relating to fixed-field inhomogeneity. In contrast, small intracellular clusters caused little SNR decrease on T2*-weighted GRE images while the small clusters produced substantial SNR loss on T2-weighted FSE images. This could attribute to T2 shortening mechanisms that were independent of magnetic susceptibility effects but relate to the greater free water interaction made possible by the relatively larger surface area of the small clusters (Tanimoto et al., 1994; Tanimoto et al., 2001). However, the size of the intracellular SPIO clusters depended on individual KC phagocytic function. Hence, impaired phagocytic activity, as in liver cirrhosis, should be associated with a decreased average size of SPIO clusters within KC. In this study, SNR of the normal liver of control rats with T2*-weighted GRE sequence decreased by about eight times on SPIO-enhanced images, while twice as that of the cirrhosis liver of model rats. This result was consistent with those reports that the signal intensity induced by SPIO in patients with liver cirrhosis was less remarkable than that in non-cirrhotic patients (Hundt et al., 2000; Clement et al., 1991; Nakayama et al., 1998). Hemangiomas could show SPIO uptake because of the blood pool effect, although they do not contain KCs (Kim et al., 2002). It was obvious that there were many iron oxide particles stainable in hemangiomas in Fig. 6. Therefore, hemangiomas could not be identified on T2*-weighted MR images.

5. Conclusion

The SPIO-alginate was cleared rapidly from serum with the half-life of 0.27 h at 109.5 μmol Fe/kg and accumulated dominantly in the liver and spleen with a total percentage of more than 90% after intravenous injection. Iron oxide particles in KCs as well as splenic red pulp were observed from histological evaluation in normal rats. The experiments on MR imaging indicated that SPIO-alginate as an MR contrast agent might have the ability to improve detection of liver tumor.

Acknowledgements

This work was supported by funds from National High Technology Research and Development Program of China (2003AA326020), National Basic Research Program of China 2007CB935801, and National Natural Science Foundation of China (30772665).

References

Bouhadir, K.H., Lee, K.Y., Alsberg, E., Damm, K.L., Anderson, K.W., Mooney, D.J., 2001. Degradation of partially oxidized alginate and its potential application for tissue engineering. Biotechnol. Prog. 17, 945–950.

Bourrinet, P., Bengele, H.H., Bonnemain, B., Dencausse, A., Idee, J.M., Jacobs, P.M., Lewis, J.M., 2006. Preclinical safety and pharmacokinetic profile of Ferumoxtran-10, an ultrasmall superparamagnetic iron oxide magnetic resonance contrast agent. Invest. Radiol. 41, 313–324.

Briley-Sæbø, K., Hustvedt, S.O., Haldorsen, A., BjØrnerud, A., 2004. Long-term imaging effects in rat liver after a single injection of an iron oxide nanoparticle based MR contrast agent. J. Magn. Reson. Imaging 20, 622–631.

Clement, O., Frija, G., Chambon, C., Schouman-Claves, E., Mosnier, J.F., Poupon, M.F., Balkau, B., 1991. Liver tumors in cirrhosis: experimental study with SPIO-enhanced MR imaging. Radiology 180, 31–36.

Corot, C., Robert, P., Idee, J.M., Port, M., 2006. Recent advances in iron oxide nanocrystal technology for medical imaging. Adv. Drug Deliv. Rev. 58, 1471–1504.

Gombotz, W.R., Wee, S.F., 1998. Protein release from alginate matrices. Adv. Drug Deliv. Rev. 31, 267–285.

Gupta, A.K., Gupta, M., 2005. Synthesis and surface engineering of iron oxide nanoparticles for biomedical applications. Biomaterials 26, 3995–4021.

Hagar, W., Vichinsky, E.P., Theil, E.C., 2003. Liver ferritin subunit ratios in neonatal hemochromatosis. Pediatr. Hematol. Oncol. 20, 229–235.

Harmut-Hoene, A., Schelenz, R., 1980. Effect of dietary fiber on mineral absorption in growing rats. J. Nutr. 110, 1774–1784.

Hauff, P., Fritzsch, T., Reinhardt, M., Weitschies, W., Lueders, F., Uhlendorf, V., Heldmann, D., 1997. Delineation of experimental liver tumors in rabbits by a new ultrasound contrast agent and stimulated acoustic emission. Invest. Radiol. 32, 94–99.

Hundt, W., Petsch, R., Helmberger, T., Reiser, M., 2000. Signal changes in liver and spleen after Endorem administration in patients with and without liver cirrhosis. Eur. Radiol. 10, 409–416.

Imai, Y., Murakami, T., Yoshida, S., Nishikawa, M., Ohsawa, M., Tokunaga, K., Murata, M., Shibata, K., Zushi, S., Kurokawa, M., Yonezawa, T., Kawata, S., Takamura, M., Nagano, H., Sakon, M., Monden, M., Wakasa, K., Nakamura, H., 2000. Superparamagnetic iron oxide-enhanced magnetic resonance images of hepatocellular carcinoma: correlation with histological grading. Hepatology 32, 205–212.

Kellar, K.E., Fujii, D.K., Gunther, W.H.H., Briley-Saebo, K., Bjornerod, A., Spiller, M., Koenig, S.H., 2002. Important considerations in the design of iron oxide nanoparticles as contrast agents for T1-weighted MRI and MRA. Acad. Radiol. 9, S34–S37.

Kellar, K.E., Fujii, D.K., Gunther, W.H.H., Briley-Saebo, K., Bjornerod, A., Spiller, M., Koenig, S.H., 2000. "NC100150 injection," a preparation of optimized iron oxide nanoparticles for positive contrast MR angiography. J. Magn. Reson. Imaging 11, 488–494.

Kim, J.H., Kim, M.J., Suh, S.H., Chung, J.J., Yoo, H.S., Lee, J.T., 2002. Characterization of focal hepatic lesions with ferumoxides-enhanced MR imaging: utility of T1-weighted spoiled gradient recalled echo images using different echo times. J. Magn. Reson. Imaging 15, 573–583.

Ma, H.L., Qi, X.R., Maitani, Y., Nagai, T., 2007. Preparation and characterization of superparamagnetic iron oxide nanoparticles stabilized by alginate. Int. J. Pharma 333, 177–186.

Ma, H.L., Qi, X.R., Ding, W.X., Maitani, Y., Nagai, T., 2007a. Magnetic targeting after femoral artery administration and biocompatibility assessment of superparamagnetic iron oxide nanoparticles. J. Biomed. Mater. Res. Part A 84A, 598–606.

Nakayama, M., Kamura, T., Kimura, M., Seki, H., Tsukada, K., Sakai, K., 1998. Quantitative MRI of hepatocellular carcinoma in cirrhotic and noncirrhotic livers. Clin. Imaging 22, 280–283.

Neuberger, T., Schöpf, B., Hofmann, H., Hofmann, M., Von Rechenberg, B., 2005. Superparamagnetic nanoparticles for biomedical applications: Possibilities and limitations of a new drug delivery system. J. Magn. Magn. Mater. 293, 483–496.

Oswald, P., Clement, O., Chambon, C., Schouman-Claeys, E., Frija, G., 1997. Liver positive enhancement after injection of superparamagnetic nanoparticles: respective role of circulating and uptaken particles. Magn. Reson. Imaging 15, 1025–1031.

Pouliquen, D., Le Jeune, J.J., Perdrisot, R., Ermias, A., Jallet, P., 1991. Iron oxide nanoparticles for use as an MRI contrast agent: pharmacokinetics and metabolism. Magn. Reson. Imaging 9, 275–283.

Reimer, P., Rummeny, E.J., Daldrup, H.E., Balzer, T., Tombach, B., Berns, T., Peters, P.E., 1995. Clinical results with resovist: a phase 2 clinical trial. Radiology 195, 489–496.

Robitaille, R., Pariseau, J.F., Leblond, F.A., Lamoureux, M., Lepage, Y., Hallé, J.P., 1999. Studies on small (<350 μm) alginate-poly-L-lysine microcapsules. III. Biocompatibility of smaller versus standard microcapsules. J. Biomed. Mater. Res. 44, 116–120.

Saini, S., Stark, D.D., Hahn, P.F., Bousquet, J.C., Introcasso, J., Wittenberg, J., Brady, T.J., Ferrucci J.T.Jr., 1987. Ferrite particles: a superparamagnetic MR contrast agent for enhanced detection of liver carcinoma. Radiology 162, 217–222.

Seternes, T., Oynebraten, I., Sorensen, K., Smedsrod, B., 2001. Specific endocytosis and catabolism in the scavenger endothelial cells of cod (*Gadus morhua* L.) generate high-energy metabolites. J. Exp. Biol. 204, 1537–1546.

Sokov, L.A., 1970. Radioaktivnye Izotopy Vo Vneshnei Sredei Organizine. Atomizdat, Moscow. p. 247.

Solandt, O.M., 1941. Some observations upon sodium alginate. Quart. J. Exp. Physiol. 31, 25–30.

Tanimoto, A., Pouliquen, D., Kreft, B.P., Stark, D.D., 1994. Effects of spatial distribution on proton relaxation enhancement by particulate iron oxide. J. Magn. Reson. Imaging 4, 653–657.

Tanimoto, A., Oshio, K., Suematsu, M., Pouliquen, D., Stark, D.D., 2001. Relaxation effects of clustered particles. J. Magn. Reson. Imaging 14, 72–77.

Tanimoto, A., Yuasa, Y., Shinmoto, H., Jinzaki, M., Imai, Y., Okuda, S., Kuribayashi, S., 2002. Superparamagetic iron oxide-mediated hepatic signal intensity change in patients with and without cirrhosis: pulse sequence effects and Kupffer cell function. Radiology 222, 661–666.

Taupitz, M., Wagner, S., Schnorr, J., Kravec, I., Pilgrimm, H., Bergmann-Fritsch, H., Hamm, B., 2004. Phase I clinical evaluation of citrate-coated monocrystalline very small superparamagnetic iron oxide particles as a new contrast medium for magnetic resonance imaging. Invest. Radiol. 39, 394–405.

Van Beers, B.E., Sempoux, C., Materne, R., Delos, M., Smith, A.M., 2001. Biodistribution of ultrasmall iron oxide particles in the rat liver. J. Magn. Reson. Imaging 13, 594–599.

Wang, Y.X., Hussain, S.M., Krestin, G.P., 2001. Superparamagnetic iron oxide contrast agents: physicochemical characteristics and applications in MR imaging. Eur. Radiol. 11, 2319–2331.

Ward, J., Guthrie, J.A., Wilson, D., Arnold, P., Lodge, P., Toogood, G.J., Wyatt, J.I., Robinson, P.J., 2003. Colorectal hepatic metastases: detection with SPIO-enhanced breath-hold MR imaging-comparison of optimized sequences. Radiology 228, 709–718.

Weinmann, H.J., Ebert, W., Misselwitz, B., Schmitt-Willich, H., 2003. Tissue-specific MR contrast agents. Eur. J. Radiol. 46, 33–44.

Weissleder, R., Stark, D.D., Engelstad, B.L., Bacon, B.R., Compton, C.C., White, D.L., Jacobs, P., Lewis, J., 1989. Superparamagnetic iron oxide: pharmacokinetics and toxicity. Am. J. Roentgenol. 152, 167–173.

Available online at www.sciencedirect.com
ScienceDirect
Journal of Controlled Release 127 (2008) 231 – 238
journal of controlled release
www.elsevier.com/locate/jconrel

In vivo antitumor activity of camptothecin incorporated in liposomes formulated with an artificial lipid and human serum albumin

Masato Watanabe [a], Kumi Kawano [a], Kazunori Toma [b], Yoshiyuki Hattori [a], Yoshie Maitani [a,*]

[a] Institute of Medicinal Chemistry, Hoshi University, Ebara 2-4-41, Shinagawa-ku, Tokyo 142-8501, Japan
[b] The Noguchi Institute, Kaga 1-8-1, Itabashi-ku, Tokyo 173-0003, Japan

Received 12 October 2007; accepted 10 February 2008
Available online 20 February 2008

Abstract

Camptothecin (CPT) is a strong antitumor agent, but its use limited by its low solubility and the instability of the active lactone form. To overcome these difficulties, liposomes incorporating CPT (CPT liposomes) were designed and tested. CPT liposomes were formulated by the addition of 3,5-bis(dodecyloxy)benzoic acid (DB) to polyethylene glycol-containing liposomes, and by coating the surface of the liposomes with human serum albumin (HSA, HSA-DB-L). HSA-DB-L successfully entrapped CPT with about 80% efficiency and with a particle size of about 150 nm. HSA-DB-L showed attenuated drug release and storage stability. Pharmacokinetics studies in mice showed that i.v. injection of HSA-DB-L (2.5 mg/kg) led to prolonged circulation in the plasma; the area under the curve was 22-fold higher than that of CPT solution. The tumor growth in mice with subcutaneous transplantation of colon 26 tumor cells was significantly inhibited after a single i.v. injection of HSA-DB-L at a dose of 15 mg/kg without any significant body weight loss. HSA-DB-L increased the accumulation of CPT in tumor tissue significantly (9.6-fold) more efficiently than CPT solution 24 h after i.v. injection. These findings suggest that HSA-DB-L could increase the stability and the antitumor effect of CPT. CPT delivery by novel liposome formulations is a potential approach for effective treatment of cancer.

Keywords: Camptothecin; Liposome; Antitumor effect; HSA; Colon 26 tumor

1. Introduction

Camptothecin (CPT) is a naturally occurring cytotoxic alkaloid isolated from the Chinese plant *Camptotheca accuminata* [1]. CPT and some of its analogs have shown a broad spectrum of antitumor activity against many solid tumors in xenografts, including colorectal cancer [2,3]. CPT inhibits the enzyme DNA topoisomerase I, initially by noncovalent binding and subsequently by stabilization of the complex through a nucleophilic attack by the enzyme at the acyl position of the CPT lactone ring [4]. Under physiological conditions, i.e., at pH 7 or above, the lactone ring readily opens to yield the inactive carboxylate form of the drug, and this conversion is in pH-dependent equilibrium [5] (Fig. 1(A)). Moreover, the presence of human serum albumin (HSA) in the blood or serum showed rapid CPT lactone ring opening. This was probably due to preferential HSA binding to the carboxylate form resulting in a change in the lactone-carboxylate equilibrium. Thus shifts the equilibrium toward the pharmacologically ineffective carboxylate form [6]. Only the lactone form of CPT is biologically active; however, this form exhibits poor aqueous solubility.

To overcome these stability and solubility problems of CPT, several approaches have been investigated. In addition to the synthesis of new derivatives and pro-drug products [7,8], the development of adequate drug carriers is gaining increasing attention. There are many reports about effective formulation and utilization of CPT in cancer therapy by using drug delivery technologies such as incorporation in liposomes [9,10], polymer micelles[11,12], microemulsions [10], and microspheres [13,14]. About liposomes, the protection of the lactone form of CPT by liposomes has been known [9]. Low solubility of CPT in water or lipids, however, was limited to develop liposomal CPT. Safer and more water-soluble CPT derivatives, therefore,

* Corresponding author. Tel./fax: +81 3 5498 5048.
E-mail address: yoshie@hoshi.ac.jp (Y. Maitani).

0168-3659/$ - see front matter © 2008 Elsevier B.V. All rights reserved.
doi:10.1016/j.jconrel.2008.02.005

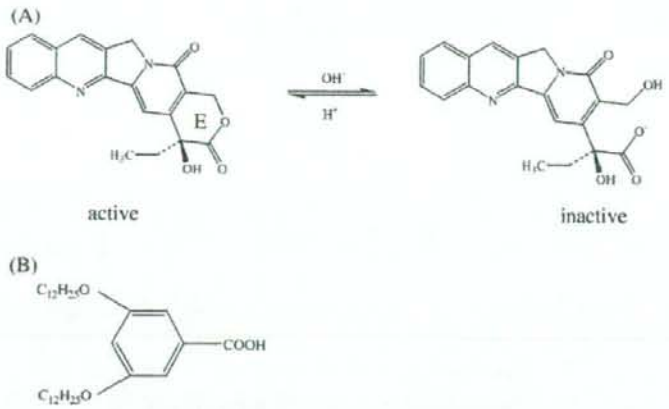

Fig. 1. Structure of camptothecin (CPT) and equilibrium reaction between the active and inactive form (A) and structure of 3,5-bis(dodecyloxy)benzoic acid (DB).

were used to be entrapped in the liposomal water phase [15,16]. CPT has higher activity than these derivatives [17]. If stable CPT liposomal formulations in vivo can be developed, high antitumor effect will be obtained.

To this purpose, novel CPT liposomes were formulated by the addition of an artificial lipid with a phenyl group to polyethylene glycol-modified liposomes, and by coating the surface of the liposomes with HSA. Because we reported that stable CPT-loaded polymer micelles in vivo were produced using benzyl polymer [11,12,18,19], presumably due to be $\pi-\pi$ interaction of the phenyl group with CPT, lipids with a phenyl group in liposomes might interact with CPT and could incorporate CPT effectively. An artificial lipid with a phenyl group, 3,5-bis (dodecyloxy) benzoic acid (DB), therefore, was synthesized (Fig. 1(B)) and added to the liposome formulation. We also modified liposomes with polyethylene glycol (PEG) for long circulating, because they can passively deliver chemotherapeutic agents to tumor sites via the enhanced permeation and retention (EPR) effect [20–22]. Furthermore, we coated the liposomes by HSA because pre-coating polystyrene particles with HSA enhanced their stability in blood [23].

In the present study, we demonstrated that CPT could be efficiently incorporated into the pegylated liposomes by the addition of DB, combined with coating HSA on the surface of the liposomes. The drug release from the liposomes, the storage stability, pharmacokinetics, and in vivo antitumor activity of HSA-DB-L were examined. The liposomal form of CPT displayed antitumor activity against mice bearing colon adenocarcinoma 26 when administered by a single i.v. injection.

2. Materials and methods

2.1. Materials

(*S*)-(+)-Camptothecin (CPT), cholesterol (Ch), high performance liquid chromatography (HPLC) grade acetonitrile and triethylamine acetate were purchased from Wako Pure Chemical Industries, Ltd. (Osaka, Japan). Hydrogenated soybean phosphatidylcholine (HSPC, >90% phosphatidylcholine), distearolyphosphatidylethanolamine-*n*-[methoxy(polyethylene glycol)-2000] (PEG2000), distearolyphosphatidylethanolamine-*n*-[methoxy(polyethylene glycol)-5000] (PEG5000) and oleic acid (OA) were purchased from NOF Corporation (Tokyo, Japan). HSA was purchased from Sigma Chemical Co. (St. Louis, MO, USA). DB was synthesized as reported previously [24]. Other chemicals were of reagent grade.

2.2. Preparation of liposomes

CPT-incorporating liposomes (CPT liposomes) composed of the formulations summarized in Table 1 were prepared by a lipid-film hydration method. Briefly, CPT (1 mg) and lipids (e.g., 30 mg of total lipids for DB-L, HSPC/Ch/OA/DB/PEG2000 = 7:3:1:1:0.4 (molar ratio) = 19.3/4.1/1.0/1.7/3.9 (mg)) were dissolved in a mixture of chloroform: methanol (4:1, volume ratio), and the solvent was removed by evaporation under nitrogen gas flow. The lipid film was hydrated with 2 mL of phosphate-buffered solution (pH 6.0, 2.33% KH_2PO_4: 1.44% $NaHCO_3$ = 4:1, volume ratio). The lipid mixture was sonicated for 30 min using an ultrasonic bath. Excess CPT was precipitated and could be separated from the liposomes by centrifugation at 1400 ×g for 10 min. Liposomes with average sizes ranging from 150 to 200 nm with low polydispersity index (<0.3) were obtained, as determined using a dynamic light scattering particle size analyzer, and surface potentials of them were determined by the electrophoresis light scattering method (ELS-800, Otsuka Electronics Co., Ltd. Osaka, Japan) at 25 °C by diluting liposome suspensions to an appropriate volume with water.

Good and reproducible recovery of liposomes in the supernatant (>80%) was obtained, as determined by an enzymatic assay using a Phospholipid C-test Wako (Wako Pure Chemical Industries, Ltd.).

Control liposomes (Control-L) were composed of HSPC, Ch, OA and PEG2000. Control-L containing 8 mol% and 15 mol% DB are hereafter designed as DB-L and 2DB-L, respectively. DB-L5000 had a similar composition as DB-L, but contained PEG5000 instead of PEG2000. For coating of DB-L with HSA (HSA-DB-L), the DB-L suspension (e.g., 7.5 mg total lipids/mL)

Table 1
Characterization of CPT liposomes

Code	Formulation (molar ratio)	Particle size (nm)	Incorporation efficiency[a] (%)	% Injected dose in plasma after 4 h[b]
CPT solution		–	–	0.02±0.01
Control-L	HSPC/Ch/OA/PEG2000 (7:3:1:0.4)	137.4±15.4	75.6±11.4	0.3±0.1
DB-L	HSPC/Ch/OA/DB/PEG2000 (7:3:1:1:0.4)	148.4±0.9	80.7±8.4	1.0±0.2
2DB-L	HSPC/Ch/OA/DB/PEG2000 (7:3:1:2:0.4)	177.2±50.5	76.9±16.9	0.04
DB-L5000	HSPC/Ch/OA/DB/PEG5000 (7:3:1:1:0.4)	148.4±0.9	85.8±4.9	0.2±0.2
HSA-DB-L	HSPC/Ch/OA/DB/PEG2000 (7:3:1:1:0.4)+HSA	161.3±9.2	85.8±4.9	2.5±0.8

Each value represents the mean±SD. ($n=3$).
*$P<0.05$, **$P<0.01$, ***$P<0.001$.
[a]Prepared at a feeding ratio of 1/30 (CPT/total lipid, w/w).
[b]Results at a dose of 2.5 mg CPT/kg in ddY mice.

was incubated with 4% HSA aqueous solution at room temperature (20–25 °C) for 1 h. HSA-DB-L was used without separation of free HSA in in vivo experiment.

The CPT solution was prepared by dissolving CPT (13.0 mg) in 50 mL of polyethylene glycol 400, propylene glycol and polysorbate 80 (40:50:2, volume ratio) [25].

2.3. Determination of HSA amount associated with HSA-DB-L

The adsorbed HSA was measured using bicinchoninic acid (BCA) protein assay reagent (Pierce, Rockford, IL, USA) and analyzed by 10% SDS-polyacrylamide gel electrophoresis (SDS-PAGE) after separation of liposomes by ultracentrifugation (100,000 ×g, 1 h, 4 °C). The gel was stained with Coomassie brilliant blue (Quick-CBB, Wako Pure Chemical Industries, Ltd., Osaka, Japan).

2.4. Cytotoxicity of liposomes containing DB

Mouse colon adenocarcinoma 26 (C26) cells (5.0×10^3 cell/well) were plated into 96-well culture plates 1 day before the experiment. The cells were incubated for 48 h at 37 °C with liposomes. The cytotoxicity was then determined using a WST-8 assay (Cell Counting Kit-8, Dojindo Laboratories, Kumamoto, Japan). The number of viable cells was determined by measuring the absorbance at 450 nm on an automated plate reader.

2.5. Determination of efficiency of CPT incorporation into liposomes

Drug incorporation efficiency was determined using the ultracentrifugation method. CPT liposomes were centrifuged at 52,000 ×g for 1 h at 4 °C to separate free CPT from liposomal CPT. Then, the incorporation efficiency was obtained using two methods: determination of the CPT concentration of the supernatant containing free CPT, and determination of the amount of CPT entrapped in the precipitate, which was disrupted using chloroform. The incorporation efficiencies estimated using both methods were similar. The former method was used in the following experiment. The total drug concentrations in liposomes before centrifugation (drug initial) and in the supernatant after centrifugation (drug supernatant) were determined using a fluorescence spectrophotometer (F-4010, Hitachi Electronics, Tokyo, Japan) with excitation and emission wavelengths of 369 and 437 nm, respectively. The percentage of the drug entrapped in the liposomes was calculated as follows:

$$\text{Incorporation efficiency (\%)} = \left(\text{drug}_{\text{initial}} - \text{drug}_{\text{supernatant}}\right)/\text{drug}_{\text{initial}} \times 100.$$

2.6. In vitro drug release of CPT liposomes

In vitro release of CPT from the liposomal formulation was analyzed by membrane dialysis against phosphate-buffered saline (PBS, pH 7.4) at 37 °C under sink condition. Briefly, 1 mL of CPT liposomes (0.4–0.5 mg CPT/mL) was placed in a dialysis tube (Spectra/Por CE, MWCO 300,000, Spectrum Laboratories, Inc., Rancho Dominguez, CA, USA) and then suspended in a temperature-controlled, jacketed flask containing 100 mL of PBS. After various time intervals, aliquots of the medium were withdrawn and assayed for CPT content by fluorophotometry.

2.7. Storage stability study

The lactone form of CPT in the HSA-DB-L was evaluated after storage at room temperature (20–25 °C) for an extended period of time. The lactone and carboxylate forms of CPT liposomes were then immediately measured by reverse-phase HPLC analysis.

The HPLC analysis was performed at room temperature. A Shimadzu LC-10AT (Shimadzu Co., Ltd., Japan) apparatus equipped with a Shimadzu RF-10AXL fluorescence detector in which the excitation and emission wavelengths were set at 369 and 437 nm, respectively, was used. Separation was performed with a Tosoh TSK-gel ODS-80Ts column (150×4.6 mm I.D.).

Table 2
Cytotoxicity of CPT liposomes to colon 26 cells

Code (formulation)	IC50 (μg/mL)
Control-L not containing CPT (HSPC/Ch/OA/PEG2000)	1.1 mg/mL*
DB-L not containing CPT (HSPC/Ch/OA/PEG2000)	1.1 mg/mL*
CPT solution	0.077
DB-L (HSPC/Ch/OA/DB/PEG2000)	0.048
HSA-DB-L (HSPC/Ch/OA/DB/PEG2000+HSA)	0.042

* Concentration of lipids.

The mobile phase was composed of 23:77 (v/v) acetonitrile-triethylamine acetate buffer (1% (v/v), adjusted to pH 5.5 with glacial acetic acid), and the flow rate was set at 1.0 mL/min [26].

2.8. Measurement of CPT concentration in plasma in mice

CPT liposomes or CPT solution was intravenously (i.v.) administered to male ddY mice (weighing 18–20 g, Tokyo Laboratory Animal Science Co., Ltd. Tokyo, Japan) via the lateral tail veins at a dose of 2.5 mg/kg (0.1–0.2 mL/10 g body weight). At various times after the administration, blood was withdrawn using a heparinized syringe and centrifuged at 15,300 ×g for 4 min to obtain the plasma. Plasma was added to 0.1 mL of 0.15 M aqueous phosphoric acid followed by mixing [27] and CPT was extracted with 0.8 mL of chloroform: methanol (4:1, volume ratio). This operation gave the total concentration of free CPT and CPT incorporated into liposomes as a lactone form. After centrifugation of the mixture at 15,300 ×g for 4 min, 25 μL of the organic solvent layer was directly injected into the HPLC system to determine the concentration of CPT. The area under the concentration curve (from 0 h to 24 h: AUC) and clearance were calculated using the bootstrap method [28].

2.9. Biodistribution studies in tumor-bearing mice

At 1 week after transplantation of 1.0×105 cells, when tumor size reached approximately 100 mm^3, C26-bearing CDF1 female mice (6 weeks old) were injected via a lateral tail vein with HSA-DB-L or CPT solution at a dose of 2.5 mg/kg as CPT. After 24 h, the mice were anesthetized with diethyl ether. Blood samples were collected and then the major organs and tumor were excised, rinsed in physiologic saline, weighed, and frozen at −20 °C. The tissues were homogenized in 5.0 mL of PBS. CPT was extracted from tissue homogenate or plasma as described above and the CPT concentration was determined by HPLC.

2.10. In vivo antitumor activity

The antitumor activity against a solid tumor was evaluated with C26. C26 cells (1.0×10^5 cells in 0.2 mL) were transplanted subcutaneously into the backs of CDF1 female mice (5 weeks old, Sankyo Labo Service Corporation, Tokyo, Japan). Drug injection was started 2 weeks after tumor transplantation, when the tumor volume reached approximately 100 mm^3 (Day 0), by i.v. injection via a lateral tail vein. CPT solution was used as a single injection at a dose of 1.5 mg/kg, and HSA-DB-L (e.g., 2.5 mg CPT and 25 mg total lipid/mL) as a single injection at a dose of 10 or 15 mg/kg, and a repeated injection of 10 mg/kg. The control group was injected with 0.9% NaCl solution (0.1 mL/10 g body weight). Tumor volumes and body weights were measured at intervals of a few days. Tumor volume was calculated as follows: volume$=1/2LW^2$; L is the long diameter and W is the short diameter of a tumor. Percent tumor growth inhibition ($T/C\%$) was calculated from the relative tumor volume at day 8 following the equation: $T/C\%=100\times$(mean relative tumor volume of treated group)/(mean relative tumor volume of control group). The animal experiments were done with ethical approval from our Institutional Animal Care and Use Committee.

2.11. Statistical analysis

The results were analyzed statistically using Student's t-test. A P-value of 0.05 or less was considered significant.

3. Results

3.1. Characterization of CPT liposomes

To obtain CPT liposomes that were stable in vivo, liposomes were prepared using various formulations by adding DB as a lipid containing a phenyl group and by coating with HSA. The use of DB as a liposome component had not previously been reported, so first the cytotoxicity of DB was evaluated in cell culture. The 50% cell growth inhibitory concentration (IC_{50}) of DB-L and Control-L not containing CPT was 1.1 mg lipid/mL, indicating that DB in liposomes was not toxic (Table 2). Furthermore, the cytotoxicity of CPT-loaded liposomes and CPT solution in DMSO was examined. IC_{50} of CPT solution, DB-L and HSA-DB-L showed 0.077, 0.048 and 0.042 μg CPT/mL. Despite of the existence of PEG2000 in liposomes, IC_{50} values of DB-L and HSA-DB-L were lower than that of CPT solution. The CPT lactone ring opened at about 20 min in medium, resulting in biological inactivity [6]. Incorporation of CPT in liposomes could maintain active lactone form even in the presence of serum, indicating that liposome formulations could keep the antitumor effect of CPT.

About Control-L, addition of PEG2000 to the liposomes increased incorporated efficiency of CPT from 30% to 75% (data not shown). The particle size and incorporation efficiency were not significantly different among all the CPT liposome formulations, and were about 150 nm and 80%, respectively.

Fig. 2. SDS-PAGE of HSA associated on the liposomes. Lane 1: HSA-DB-L (HSPC/Ch/OA/DB/PEG2000+HSA), Lane 2: HSA-DB-L without PEG2000 (HSPC/Ch/OA/DB+HSA).

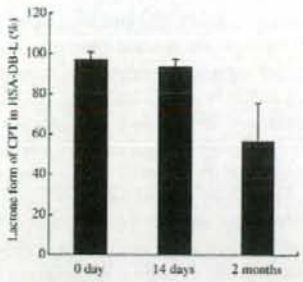

Fig. 3. Storage stability of lactone form of CPT incorporated in HSA-DB-L at room temperature. Each value represents the mean±SD. ($n=3$).

when the liposomes were prepared at a feeding ratio of 1/30 (w/w) CPT/total lipid (Table 1). The effect of PEG on the association of HSA was evaluated using HSA-DB-L with or without PEG2000. The adsorbed HSA amounts on HSA-DB-L (HSPC/Ch/OA/DB/PEG2000+HSA) and HSA-DB-L without PEG2000 (HSPC/Ch/OA/DB+HSA) was 58.7±5.3 and 73.3±6.5 mg HSA/g HSPC, respectively. The presence of PEG reduced the association of HSA on the surface of DB-L compared with DB-L without PEG2000. This finding was also confirmed by SDS-PAGE as shown in Fig. 2. HSA-DB-L was successfully modified with HSA by incubation.

Moreover, analysis of HSA-DB-L, i.e., DB-L coated with HSA, demonstrated that neither the particle size nor the incorporation efficiency was changed by incubation of the liposomes with HSA. The surface potentials of DB-L and HSA-DB-L were −23.1±2.0 mV and −26.3±5.4 mV, respectively.

Drug release profiles of Control-L and DB-L showed that there was approximately 30% drug release from CPT liposomes into PBS over 72 h (data not shown), suggesting the CPT remained associated with the liposomes during the course of the study. This finding also suggests that CPT liposomes would be stable in dilute conditions.

3.2. In vivo circulation stability of CPT liposomes

To determine whether CPT liposomes were stable and long circulating, the plasma concentration of CPT liposomes was evaluated 4 h after mice were injected intravenously (Table 1). DB-L, which contained DB in addition to the formulation of Control-L, showed a significantly (about 3-fold) higher level CPT in the plasma compared to Control-L ($P<0.05$). This suggests that the addition of DB in the liposome bilayer increased the stability of CPT-incorporating liposomes in the blood. However, changing the PEG length from 2000 to 5000 (DB-L5000) or the addition of a 2-fold larger amount of DB in DB-L (2DB-L) failed to increase the CPT plasma concentration, although both formulations showed similar particle size and incorporation efficiency as DB-L. The result suggests that the level of incorporation of DB influenced on the distribution of CPT in liposomes.

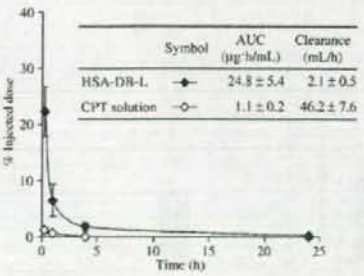

Fig. 4. Plasma concentration–time curves of the HSA-DB-L and CPT solution following i.v. injection at a dose of 2.5 mg CPT/kg in ddY mice. Each value represents the mean±SD. ($n=3$).

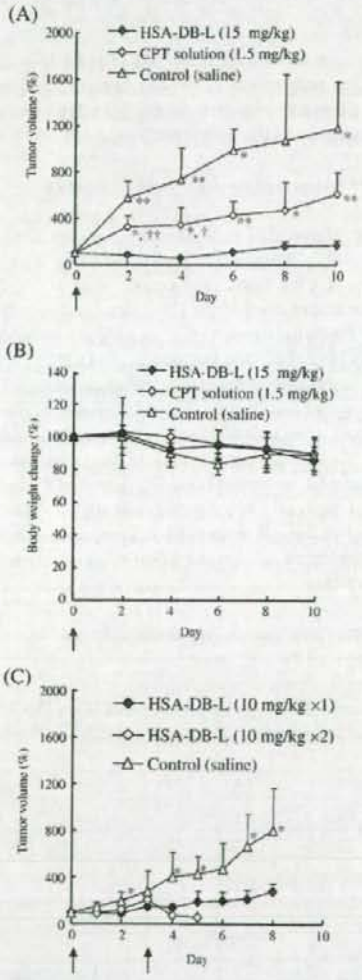

Fig. 5. In vivo antitumor activity in mice bearing C26 tumors. (A, B) Tumor volume and body weight change after a single injection of 15 mg/kg CPT in HSA-DB-L or 1.5 mg/kg CPT solution. (C) Single or repeated injection of 10 mg/kg CPT in HSA-DB-L. Arrows indicate the day of drug injections. Tumor volumes are plotted as ratios to their volume prior to the first drug injection. Each value represents the mean±S.D. ($n=4$) *$P<0.05$, **$P<0.01$ compared with HSA-DB-L, †$P<0.05$, ††$P<0.01$ compared with control.

It has been reported that pre-coating polystyrene particles with HSA enhanced their stability in blood [23]. To increase the circulation stability of DB-L, therefore, the surface of DB-L was coated with HSA (HSA-DB-L). HSA-DB-L showed significantly (about 2.5-fold) higher CPT plasma concentration than DB-L ($P<0.01$).

3.3. Storage stability of CPT liposomes

Generally, the carboxylate form of CPT binds with HSA and is changed to the pharmacologically ineffective carboxylate form [5]. Therefore, the storage stability of HSA-DB-L at room temperature was examined by measuring the amount of CPT lactone form remaining by HPLC. As shown in Fig. 3, more than 95% of the lactone form of CPT in HSA-DB-L remained 14 days after preparation ($P>0.05$), and more than 50% at 2 months compared with that on day 0 without change of the size/polydispersity index over time.

3.4. Plasma concentration–time profiles in mice

As shown above, CPT liposomes that were stable in the blood circulation and in storage were obtained using an appropriate formulation of CPT liposomes coated with HSA. Next, the plasma pharmacokinetics of the HSA-DB-L was compared with these of CPT solution in mice (Fig. 4). CPT solution disappeared very quickly from the blood circulation. The CPT in HSA-DB-L was clearly more stable in the blood circulation than CPT solution. The percentage of the injected dose of HSA-DB-L remaining in plasma 15 min, 1, and 4 h after injection was significantly (19.5-, 10.9-, and 44.5-fold, respectively) higher than that of CPT solution. The AUC values of HSA-DB-L and CPT solution were 24.8 and 1.1 μg·h/mL, respectively, and their clearance values were 2.1 and 46.2 mL/h, respectively. Thus, HSA-DB-L showed about 22-fold higher AUC and a 22-fold lower clearance values than CPT solution.

3.5. Efficacy of single or repeated administration of CPT liposomes in C26-bearing mice

The efficacy of a single i.v. injection of HSA-DB-L at a dose of 15 mg CPT/kg against the growth of C26 in tumor-bearing mice was evaluated by monitoring tumor growth (Fig. 5(A)). The dose of CPT liposomes was decided from data that CPT-loaded polymeric micelles showed the maximum dose was 30 mg/kg after a single i.v. administration to mice [12]. HSA-DB-L showed much higher antitumor activity than CPT solution or the saline control. Mice treated with CPT solution showed a significantly smaller tumor volume than control mice. The relative tumor volume (%) in HSA-DB-L-treated mice was significantly lower than that in mice treated with the saline control or CPT solution with treated/control (T/C) volume of 16.4% at Day 8. The mice treated with HSA-DB-L as a single i.v. injection at a dose of 15 mg CPT/kg did not show any significant body weight loss during the observation period (Fig. 5(B)). The dose of CPT solution used (1.5 mg CPT/kg) was 10-fold lower than that of HSA-DB-L. The dose could not be increased, because in preliminary experiments a higher dose (2.5 mg/kg) often resulted in death after i.v. injection. Thus, the antitumor treatment with HSA-DB-L would have yielded a higher plasma concentration of CPT, and this may have accounted for the larger antitumor effect than that of CPT solution.

In order to increase the efficacy of the treatment using HSA-DB-L, the administration schedule was changed to repeated injection using a decreased dose (10 mg/kg instead of 15 mg/kg) on Days 0 and 3 (Fig. 5(C)). A single injection of HSA-DB-L at a dose of 10 mg CPT/kg showed significant antitumor activity with T/C% of 34.6 at Day 8. Repeated injection of HSA-DB-L resulted in a body weight loss of approximately 20% on the third day after the second injection (data not shown), and within 2 more days, all of the treated mice died. This seemed to be related to CPT toxicity, because when empty HSA-DB-L (not containing CPT) was injected in mice on the same schedule as used in Fig. 5(C), no mice died (data not shown).

3.6. Biodistribution of CPT liposomes in tumor-bearing mice

Fig. 6(A) shows the amount of CPT in tissues of mice bearing C26 tumors, and Fig. 6(B) shows the percent of the dose of injected CPT in the blood 24 h after the injection of HSA-DB-L. Tumor tissue exposed to HSA-DB-L demonstrated significantly (9.6-fold) higher CPT accumulation than tumor tissue exposed to CPT solution ($P<0.05$). CPT accumulation of HSA-DB-L in liver and lung was decreased but that of kidneys was increased

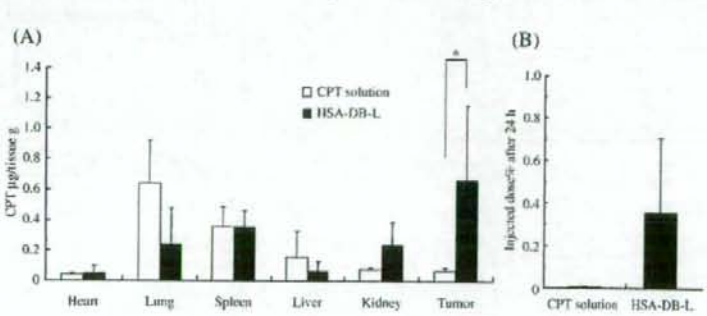

Fig. 6. Biodistribution of CPT 24 h after i.v. injection of HSA-DB-L or CPT solution (2.5 mg CPT/kg) into mice bearing C26. (A) Amount CPT per tissue weight. Each value represents the mean±S.D. ($n=3$) *: $P<0.05$ (B) % of injected dose of CPT in plasma. Each value represents the mean±S.E. ($n=3$).

by HSA-DB-L treatment ($P>0.05$). Furthermore, the plasma level of CPT in HSA-DB-L-treated mice remained 60-fold higher than that in mice treated with CPT solution.

4. Discussion

Stable pegylated liposome-incorporated CPT was obtained by the addition of DB to the formulation for liposomes combined with coating the surface of the liposomes with HSA. The CPT liposomes showed activity against C26 tumors resulting from high accumulation of CPT in the tumors when administered as a single i.v. injection in mice.

To improve the pharmacological usefulness of CPT, a liposomal formulation including CPT was developed, and the CPT liposomes were evaluated regarding their particle size, incorporation efficiency, drug release in vitro, and stability in vivo. Liposomes composed of HSPC and Ch showed low retention in the blood 4 h after injection (0.09% of injected dose of CPT). Addition of OA to the liposomes increased the retention of the injected dose of CPT to 0.4% (data not shown), suggesting that OA might increase the acidity of liposomes, resulting in stabilization of the lactone form of CPT.

All formulations demonstrated high incorporation efficiency (more than about 80%) when liposomes were prepared in acidic conditions (pH 6.0) (Table 1). This could be due to the fact that the stability of the lactone form of the CPT molecule is favored by lower pH conditions than the carboxylate form, which is more hydrophilic at pH 7.0 [29]. Among the formulations examined, DB-L (HSPC/Ch/OA/DB/PEG2000 7:3:1:1:0.4) was most stable after i.v. injection. At present, whether DB interacts with CPT is not clear, but we have reported that the stability of CPT-loaded polymeric micelles in vivo was increased by benzyl esterification of the hydrophobic segment of the block copolymer [11], presumably due to be $\pi-\pi$ interaction of the phenyl group with CPT. DB in liposome membranes, therefore, might interact with CPT by a $\pi-\pi$ interaction and could incorporate CPT into the interior of the bilayers. However, 2DB-L, containing 15 mol% DB, decreased the CPT concentration in plasma compared to DB-L. This suggests that there is an optimal amount of DB for increasing the stability of CPT liposomes, which may be between 8 and 15 mol%. As mentioned above, CPT interacted with DB in liposomal membrane. The incorporation efficiency of DB in liposomes had optimal value. Thus, optimal amount of DB for increasing CPT stability may exist.

The association of some serum protein with opsonic activity has been suppressed in previous studies by pre-coating HSA on the surface of nanoparticles and nanospheres [23,30]. In accord with those observations, HSA-DB-L increased the stability of CPT in the circulation compared to liposomes without HSA on their surface. Carbonyl group of the ring D of CPT may be in liposomes and HSA coating may stabilize them.

CPT solution given as a single i.v. injection at 2.5 mg/kg in tumor-bearing mice often resulted in toxic death, but HSA-DB-L at 15 mg/kg did not cause any significant body weight loss. This finding suggests that HSA-DB-L was up to 6 times less toxic than CPT solution administered by i.v. injection. The pharmacokinetics and tissue distribution data indicated that this reduced toxicity was attributable to lower uptake of CPT in the liver and lung after treatment with HSA-DB-L than after the administration of an equimolar dose of CPT solution. Because of this reduced toxicity, a higher dose of CPT liposomes could be used to treat mice bearing murine colon cancer. HSA-DB-L with low clearance increased the accumulation of CPT in tumor tissue, resulting in increase of the antitumor effect of CPT.

Regarding the therapeutic strategy, it has been shown in nude mice bearing human tumor xenografts that for a fixed total dose, repeated daily administration of CPT conjugated with polymers was far superior to a single injection [31]. Here, our findings suggest that a single injection of HSA-DB-L was effective for suppressing tumor growth at a dose of either 10 or 15 mg/kg ($T/C\%=34.6\%$ and 16.4% at Day 8, respectively). This apparent discrepancy may be due to a difference in the rate of release of free CPT from the liposomes. Although CPT has been shown to be released slowly from CPT conjugated with polymers over several days [31,32], HSA-DB-L released about 20% of its load within 24 h from release test into PBS. These findings suggest that the rapid bioavailability of free CPT from the liposomes may indeed improve antitumor activity subsequent to the passive accumulation of liposomes in the tumor tissue.

DB was not cytotoxic, and therefore the antitumor effect of HSA-DB-L may have been due to CPT. Furthermore, we have synthesized DB derivatives and investigated the interaction between the dodecyloxy group of DB and the lactone ring of CPT to estimate the distribution of CPT in liposomes containing DB. These results were reported as separate manuscript [33].

The results from the biodistribution study revealed that the intravenously injected HSA-DB-L accumulated in the tumor. Drug carriers with a prolonged circulation time can increase the drug accumulation in tumor tissues by the EPR effect, and consequently improve the antitumor activity. Although pegylated liposome, HSA-DB-L seemed to contribute improved CPT solubility in lipids over long circulating, these results suggest that HSA-DB-L with stable property in blood possesses the ability to deliver large amounts of CPT to the tumor site. Here further studies with human tumor xenografts will be required to evaluate the activity of HSA-DB-L.

5. Conclusion

CPT liposomes formulated with DB increased the CPT stability in vitro and in vivo. Furthermore, CPT liposomes coated with HSA prolonged the blood circulation time. This formulation enhanced the accumulation of CPT in tumor tissue, resulting in a significantly higher antitumor effect than CPT solution even with a single injection. This finding will permit the utilization of CPT, which is not now used in clinical practice due to the lack of a suitable drug carrier system.

Acknowledgements

This study was supported in part by the Ministry of Education, Culture, Sports, Science and Technology, Japan, and by the Open Research Center Project. We are grateful to Ms. S. Katayama, Ms. C. Fujita and Ms. M. Katori for technical assistance.

References

[1] M.E. Wall, M.C. Wani, C.E. Cook, K.H. Palmer, A.T. Mcphail, G.A. Sim, Plant antitumor agents: I. The isolation and structure of camptothecin, a novel alkaloidal leukemia and tumor inhibitor from Camptotheca acuminate, J. Am. Chem. Soc. 88 (1966) 3888–3890.

[2] B.C. Giovanella, J.S. Stehlin, M.E. Wall, M.C. Wani, A.W. Nicholas, L.F. Liu, R. Silber, M. Potmesil, DNA topoisomerase I-targeted chemotherapy of human colon cancer in xenografts, Science 246 (1989) 1046–1048.

[3] B.C. Giovanella, H.R. Hinz, A.J. Kozielski, J.S. Stehlin Jr., R. Silber, M. Potmesil, Complete growth inhibition of human cancer xenografts in nude mice by treatment with 20-(*S*)-camptothecin, Cancer Res. 51 (1991) 3052–3055.

[4] R.P. Hertzberg, M.J. Caranfa, S.M. Hecht, On the mechanism of topoisomerase I inhibition by camptothecin: evidence for binding to an enzyme–DNA complex, Biochemistry 28 (1989) 4629–4638.

[5] J. Fassberg, V.J. Stella, A kinetic and mechanistic study of the hydrolysis of camptothecin and some analogues, J. Pharm. Sci. 81 (1992) 676–684.

[6] Z. Mi, T.G. Burke, Differential interactions of camptothecin lactone and carboxylate forms with human blood components, Biochemistry 33 (1994) 10325–10336.

[7] K. Akimoto, A. Kawai, K. Ohya, Kinetic studies of the hydrolysis and lactonization of camptothecin and its derivatives, CPT-11 and SN-38, in aqueous solution, Chem. Pharm. Bull. 42 (1994) 2135–2138.

[8] B.A. Hanson, R.L. Schowen, V.J. Stella, A mechanistic and kinetic study of the E-ring hydrolysis and lactonization of a novel phosphoryloxymethyl prodrug of camptothecin, Pharm. Res. 20 (2003) 1031–1038.

[9] T.G. Burke, A.E. Staubus, A.K. Mishra, Liposomal stabilization of camptothecin's lactone ring, J. Am. Chem. Soc. 114 (1992) 8318–8319.

[10] R. Cortesi, E. Esposito, A. Maietti, E. Menegatti, C. Nastruzzi, Formulation study for the antitumor drug camptothecin: liposomes, micellar solution, and a microemulsion, Int. J. Pharm. 159 (1997) 95–103.

[11] M. Watanabe, K. Kawano, M. Yokoyama, P. Opanasopit, T. Okano, Y. Maitani, Preparation of camptothecin-loaded polymeric micelles and evaluation of their incorporation and circulation stability, Int. J. Pharm. 308 (2006) 183–189.

[12] K. Kawano, M. Watanabe, T. Yamamoto, M. Yokoyama, P. Opanasopit, T. Okano, Y. Maitani, Enhanced antitumor effect of camptothecin loaded in long-circulating polymeric micelles, J. Control. Release 112 (2006) 329–332.

[13] A. Shenderova, T.G. Burke, S.P. Schwendeman, The acidic microclimate in poly(lactide-co-glycolide) microspheres stabilizes camptothecins, Pharm. Res. 16 (1999) 241–248.

[14] W. Tong, L. Wang, M.J. D'Souza, Evaluation of PLGA microspheres as delivery system for antitumor agent-camptothecin, Drug Dev. Ind. Pharm. 29 (2003) 745–756.

[15] G.T. Colbern, D.J. Dykes, C. Engbers, R. Musterer, A. Hiller, E. Pegg, R. Saville, S. Weng, M. Luzzio, P. Uster, M. Amantea, P.K. Working, Encapsulation of the topoisomerase I inhibitor GL147211C in pegylated (STEALTH) liposomes: pharmacokinetics and antitumor activity in HT29 colon tumor xenografts, Clin. Cancer Res. 4 (1998) 3077–3082.

[16] C.L. Messerer, E.C. Ramsay, D. Waterhouse, R. Ng, E.M. Simms, N. Harasym, P. Tardi, L.D. Mayer, M.B. Bally, Liposomal irinotecan: formulation development and therapeutic assessment in murine xenograft models of colorectal cancer, Clin. Cancer Res. 10 (2004) 6638–6649.

[17] A. Tanizawa, A. Fujimori, Y. Fujimori, Y. Pommier, Comparison of topoisomerase I inhibition, DNA damage, and cytotoxicity of camptothecin derivatives presently in clinical trials, J. Natl. Cancer Inst. 86 (1994) 836–842.

[18] M. Yokoyama, P. Opanasopit, T. Okano, K. Kawano, Y. Maitani, Polymer design and incorporation methods for polymeric micelle carrier system containing water-insoluble anti-cancer agent camptothecin, J. Drug Target. 12 (2004) 373–384.

[19] P. Opanasopit, M. Yokoyama, M. Watanabe, K. Kawano, Y. Maitani, T. Okano, Block copolymer design for camptothecin incorporation into polymeric micelles for passive tumor targeting, Pharm. Res. 21 (2004) 2001–2008.

[20] Y. Matsumura, H. Maeda, A new concept for macromolecular therapeutics in cancer chemotherapy: mechanism of tumoritropic accumulation of proteins and the antitumor agent smancs, Cancer Res. 46 (1986) 6387–6392.

[21] H. Maeda, The enhanced permeability and retention (EPR) effect in tumor vasculature, The key role of tumor-selective macromolecular drug targeting, Adv. Enzyme Regul. 41 (2000) 189–207.

[22] H. Maeda, J. Wu, T. Sawa, Y. Matsumura, K. Hori, Tumor vascular permeability and the EPR effect in macromolecular therapeutics: a review, J. Control. Release 65 (2000) 271–284.

[23] K. Ogawara, K. Furumoto, S. Nagayama, K. Minato, K. Higaki, T. Kai, T. Kimura, Pre-coating with serum albumin reduces receptor-mediated hepatic disposition of polystyrene nanosphere: implications for rational design of nanoparticles, J. Control. Release 100 (2004) 451–455.

[24] V.S.K. Balagurusamy, G. Ungar, V. Percec, G. Johansson, Rational design of the first spherical supramolecular dendrimers self-organized in a novel thermotropic cubic liquid-crystalline phase and the determination of their shape by X-ray analysis, Am. Chem. Soc. 119 (1997) 1539–1555.

[25] S.C. Yang, L.F. Lu, Y. Cai, J.B. Zhu, B.W. Liang, C.Z. Yang, Body distribution in mice of intravenously injected camptothecin solid lipid nanoparticles and targeting effect on brain, J. Control. Release 59 (1999) 299–307.

[26] D.L. Warner, T.G. Burke, Simple and versatile high-performance liquid chromatographic method for the simultaneous quantitation of the lactone and carboxylate forms of camptothecin anticancer drugs, J. Chromatogr. B Biomed. Sci. Appl. 691 (1997) 161–171.

[27] H. Onishi, Y. Machida, Y. Machida, Antitumor properties of irinotecan-containing nanoparticles prepared using poly(DL-lactic acid) and poly (ethylene glycol)-block-poly(propylene glycol)-block-poly(ethylene glycol), Biol. Pharm. Bull. 26 (2003) 116–119.

[28] S. Takemoto, K. Yamaoka, M. Nishikawa, Y. Takakura, Histogram analysis of pharmacokinetic parameters by bootstrap resampling from one-point sampling data in animal experiments, Drug Metab Pharmacokinet 21 (2006) 458–464.

[29] R.P. Hertzberg, M.J. Caranfa, K.G. Holden, D.R. Jakas, G. Gallagher, M.R. Mattern, S.M. Mong, J.O. Bartus, R.K. Johnson, W.D. Kingsbury, Modification of the hydroxy lactone ring of camptothecin: inhibition of mammalian topoisomerase I and biological activity, J. Med. Chem. 32 (1989) 715–720.

[30] V.P. Torchilin, V.R. Berdichevsky, A.A. Barsukov, V.N. Smirnov, Coating liposomes with protein decreases their capture by macrophages, FEBS Lett. 111 (1980) 184–188.

[31] Y. Zou, Q.P. Wu, W. Tansey, D. Chow, M.C. Hung, C. Charnsangavej, S. Wallace, C. Li, Effectiveness of water soluble poly(L-glutamic acid)-camptothecin conjugate against resistant human lung cancer xenografted in nude mice, Int. J. Oncol. 18 (2001) 331–336.

[32] M. Zamai, M. VandeVen, M. Farao, E. Gratton, A. Ghiglieri, M.G. Castelli, E. Fontana, R. D'Argy, A. Fiorino, E. Pesenti, A. Suarato, V.R. Caiolfa, Camptothecin poly[*n*-(2-hydroxypropyl) methacrylamide] copolymers in antitopoisomerase-I tumor therapy: intratumor release and antitumor efficacy, Mol. Cancer Ther. 2 (2003) 29–40.

[33] Y. Maitani, S. Katayama, K. Kawano, A. Hayama, K. Toma, Artificial lipids stabilized camptothecin incorporated into liposomes, Biol. Pharm. Bull. (in press).

Artificial Lipids Stabilized Camptothecin Incorporated in Liposomes

Yoshie MAITANI,*[a] Sayaka KATAYAMA,[a] Kumi KAWANO,[a] Akihiro HAYAMA,[a] and Kazunori TOMA[b]

[a] *Institute of Medicinal Chemistry, Hoshi University; Shinagawa-ku, Tokyo 142–8501, Japan: and* [b] *The Noguchi Institute; Itabashi-ku, Tokyo 173–0003, Japan.*

Received October 31, 2007; accepted February 12, 2008; published online February 13, 2008

Camptothecin (CPT) has anticancer activity. While only the lactone form of CPT is biologically active, this form exhibits poor aqueous solubility. Pharmaceutical formulation of CPT incorporated in liposomes is of significant importance to develop the therapeutic utilization of CPT. The aim of this study was to increase incorporation efficiency and stability of CPT in liposomes composed of hydrogenated soybean phosphatidylcholine, cholesterol, and oleic acid (7 : 3 : 1, molar ratio), by incorporating three kinds of artificial lipids (DBs) (DB-liposome); 4-*n*-(M12B), 3,5-bis(B12B) and 3,4,5-tris(dodecyloxy)benzoic acid (T12B). The interaction of CPT with DB in the state of liposomes, was examined. In DB-liposomes presenting mean diameters of 150 nm, incorporation efficiency of CPT up to 55% and final drug to lipid molar ratio up to 0.07 were obtained when the liposomes were prepared at a feeding ratio of 1/30 (w/w) CPT/total lipid. However, in the optimal formulations, incorporated DB mol% was different; T12B and D12B were incorporated about one third and half mol% of M12B, respectively. Moreover, we demonstrated that T12B stabilized CPT in liposomes significantly compared with other DBs as measured by CPT release, and by steady state fluorescence polarization degree of CPT using intrinsic fluorescence of CPT. These findings suggested that in addition of contribution of phenyl group of DB, dodecyloxy group may interact strongly with lactone ring of CPT. The capacity to contain CPT interacted with DBs may be limited in liposomes. T12B may be incorporated in the interior of the bilayers, resulting in increase of incorporation stability of CPT. This finding demonstrates a potential application of the novel liposome formulation of CPT in drug delivery.

Key words camptothecin; liposome; artificial lipid; release test; incorporation efficiency; incorporation stability

Camptothecin (CPT) is a naturally occurring cytotoxic alkaloid isolated from the Chinese plant *Camptotheca accuminate*.[1] CPT and some of its analogs have shown a broad spectrum of antitumor activity against many solid tumors in xenografts including colorectal cancer.[2,3] CPT inhibits the enzyme DNA topoisomerase I, initially by noncovalent binding and subsequently by stabilization of the complex through a nucleophilic attack by the enzyme at the acyl position of the CPT lactone ring.[4]

Of significant importance for pharmaceutical formulation is that, while only the lactone form of CPT is biologically active, this form exhibits poor aqueous solubility. The lactone of CPT is converted to carboxylate in a pH-dependent equilibrium.[5] To overcome the aforementioned solubility problems and hydrolytic processes of CPT, several approaches have been investigated. Numerous attempts have been made to prepare water-soluble CPT analogs. The majority of these analogs were less potent in assays both *in vitro* and *in vivo* than the parent drug. In addition to the synthesis of new derivatives and pro-drug products,[6—10] the development of adequate drug carriers is gaining increasing attention. There are many reports about effective formulation and utilization of CPT in cancer therapy by using drug delivery technologies such as liposomes,[11,12] microemulsions,[12] microspheres,[13,14] and inclusion complexes with cyclodextrins.[15] Previously we have reported that the stability of CPT loaded polymeric micelles *in vivo* was increased by benzyl esterification of hydrophobic segment of block copolymer.[16—18] However, long circulation of CPT loaded polymeric micelles *in vivo* was not achieved yet. Other carriers such as liposomes were examined because release of drugs encapsulated in carriers depended on carriers. The designed amphipathic compounds are called artificial lipid, which has similar properties with phospholipid to form vesicles. Therefore, artificial lipid with a phenyl group, *e.g.*, 3,5-bis(dodecyloxy)benzoic acid, was synthesized and added to the liposome formulation. The PE-Gylated liposomes incorporating CPT were stable *in vivo*.[19] However, there was not enough information about interaction between CPT and artificial lipid molecules in liposomes.

To develop the therapeutic utilization of CPT, it is necessary to prepare liposomes with high incorporation efficiency and stability of CPT. This study demonstrated that incorporation of 5 mol% of 3,4,5-tris(dodecyloxy)benzoic acid increased incorporation efficiency and stability of CPT in liposomes.

MATERIALS AND METHODS

Materials (*S*)-(+)-Camptothecin (CPT), cholesterol (Ch), high performance liquid chromatography (HPLC) grade methanol and tetrahydrofuran (THF) were purchased from Wako Pure Chemicals (Tokyo, Japan). Hydrogenated soybean phosphatidylcholine (HSPC, >90% phosphatidylcholine), and oleic acid (OA) were purchased from NOF Corporation (Tokyo, Japan). 4-*n*-Dodecyloxy benzoic acid (M12B) was purchased from Tokyo Chemical Industry (Tokyo, Japan). 3,5-Bis(dodecyloxy)benzoic acid (B12B) and 3,4,5-tris(dodecyloxy)benzoic acid (T12B) were synthesized as reported previously[20] (Fig. 1). Other chemicals were of reagent grade.

Preparation of Liposomes Liposomes incorporating CPT were prepared as described elsewhere.[19] Briefly, HSPC, Ch, OA, DB and CPT (molar ratio, HSPC : Ch : OA : DB : CPT = 7 : 3 : 1 : 0—3 : 1; weight ratio, total lipid : CPT = 30 : 1) were dissolved in methanol/chloroform mixture (1/4 (v/v)). The solvent was evaporated in a rotary evaporator at 55 °C under stream of N_2 gas. The lipid film containing the drug was hydrated with 2.5 ml of sodium phosphate-buffered solu-

* To whom correspondence should be addressed. e-mail: yoshie@hoshi.ac.jp

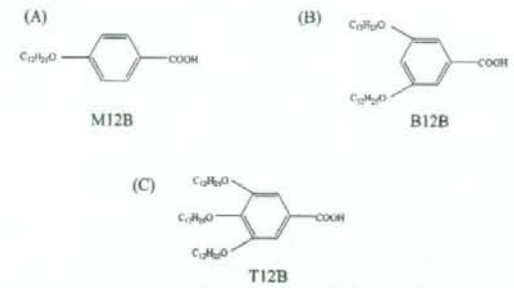

Fig. 1. Chemical Structure of 4-*n*-Dodecyloxy Benzoic Acid (A), 3,5-Bis(dodecyloxy)benzoic Acid (B), and 3,4,5-Tris(dodecyloxy)benzoic Acid (C)

tion (pH 6.04, 2.33% KH_2PO_4: 1.44% $NaHCO_3$=4:1 volume ratio) to protect conversion from the lactone of CPT to carboxylate. The suspension was sonicated for 8 min and was concentrated by centrifugation at 3900 rpm for 10 min to remove the big particles including unentrapped CPT aggregate. Size distribution of liposomes was monitored using a dynamic light scattering particle size analyzer (ELS-800, Otsuka Electronics, Osaka, Japan) at 25 °C by diluting liposome suspensions to an appropriate volume with water.

Determination of CPT and DB Content in Liposomes Drug incorporation efficiency was determined using the ultra-centrifugation method. Liposomes incorporating CPT were centrifuged at 52000 ***g*** for 1 h at 4 °C to separate free CPT. Then, the incorporation efficiency was obtained using two methods: determination of the CPT concentration of the supernatant containing free CPT, and determination of the amount of CPT entrapped in the precipitate, which was disrupted using chloroform. The incorporation efficiencies estimated using both methods were similar. The former method was used in the following experiment. The total drug concentrations in liposomes before centrifugation (liposome A) and in the supernatant after centrifugation (supernatant B) were determined using a F-4010 fluorescence spectrophotometer (Hitachi Electronics, Tokyo, Japan) with the excitation and emission wavelengths of 369 and 437 nm, respectively as described previously.[16]

Incorporation efficiency of DB was determined by HPLC (wavelength at 254 nm). A Shimadzu LC-10AT (Shimadzu Co., Ltd., Japan) apparatus equipped with a Shimadzu RF-10AXL fluorescence detector in which the wavelengths were set at 254 nm. Separation was performed with an YMC-Pack ODS-AA-302 column (150×4.6 mm I.D., YMC Co., Ltd., Kyoto, Japan). For M12B and B12B, the mobile phase was composed of 19:1 or 99:1 methanol–phosphate-buffered solution (pH 3.02), respectively, and the flow rate was set at 1.0 ml/min. For T12B, 17:3 (v/v) methanol–THF. The incorporation efficiency of drug or DB in the liposomes was calculated as follows.

$$\text{incorporation efficiency of drug or DB (\%, w/w)} = \frac{\text{drug (DB)}_{\text{liposome A}} - \text{drug (DB)}_{\text{supernatant B}}}{\text{drug (DB)}_{\text{initial}}} \times 100$$

***In Vitro* Drug Release** *In vitro* release of CPT from the liposomal formulation was analyzed by membrane dialysis against phosphate-buffered saline (PBS, pH 7.4) at 37 °C. Briefly, 1 ml of CPT liposomes was placed in a dialysis tube (Spectra/Por CE (MWCO 12000—14000, Spectrum Laboratories, Inc., Rancho Dominguez, CA, U.S.A.)) and then suspended in a temperature-controlled, jacketed flask containing 100 ml of PBS. After various time intervals, aliquots were withdrawn and assayed for CPT content by fluorophotometry. Drug release profiles (percent release *versus* time) were plotted.

Fluorescence Polarization Measurements To evaluate distribution of CPT in the liposomes, we examined mobility of CPT using intrinsic fluorescence of CPT by fluorescence polarization measurements. We prepared about 10 μM of lipid concentration of M12B-, B12B- and T12B-liposome (HSPC: Ch: OA: M12B: CPT=7:3:1:1:x, HSPC: Ch: OA: B12B: CPT=7:3:1:1:x, and HSPC: Ch: OA: T12B: CPT=7:3:1:1:x, molar ratio) aqueous suspension with CPT concentration varied from 5.7×10^{-1} μg/ml to 0.1 mg/ml (corresponding on x molar ratio). Steady-state fluorescence polarization measurements were performed on F-4500 fluorescence spectrophotometer (HITACHI, Electronics). One-centimeter rectangular quartz fluorometer cell was used, and the excitation and emission wavelengths were set at 369 and 437 nm, respectively. The fluorescence polarization of liposomes in sodium phosphate-buffered solution (pH 6.04) was measured at room temperature (24 °C). $I_{\parallel}$ ($I_{\perp}$) is the intensity of photons with electric vectors parallel (perpendicular) to the beam direction.

$$\text{polarization degree} = \frac{I_{\parallel} - I_{\perp}}{I_{\parallel} + I_{\perp}}$$

Statistical Analysis The statistical significance of the data was evaluated with Student's t test. A p value of 0.05 or less was considered significant.

RESULTS AND DISCUSSION

Preparation and Characterization of CPT Incorporated in Liposomes The incorporation stability of CPT in polymeric micelles *in vitro* and *in vivo* was increased by benzyl esterification of hydrophobic segment of block copolymer, supposed to be π–π interaction of phenyl group with CPT.[16—19] Therefore, the artificial lipids with a phenyl group, DBs were synthesized and added to liposome formulation to obtain stable liposomes incorporating CPT (DB-liposome). Basic formulation, HSPC: Ch: OA: CPT=7:3:1:1 (molar ratio) was decided as HSPC, Ch and OA since liposomes with OA showed about five-fold higher incorporation efficiency of CPT compared with ones without OA.[19] Here we prepared three kinds of liposomes incorporating M12B, B12B and T12B, referred as M12B-, B12B-, and T12B-liposome, respectively. The particle size was not significantly different among all the DB-liposome formulations, and was about 150 nm, when the liposomes were prepared at a feeding ratio of 1/30 CPT/total lipid.

Effect of DB/lipid Ratio on Incorporation to Liposomes CPT and DB contents in liposomes were determined at liposome formulation as HSPC: Ch: OA: DB: CPT=7:3:1:0—3:1 (mol), as shown in Figs. 2 and 3. When the ratio of each DB to starting total lipid of M12B-, B12B- and T12B-liposomes was increased to 15.3 mol%, the incorporation efficiency of M12B, B12B and T12B was increased to 84, 61

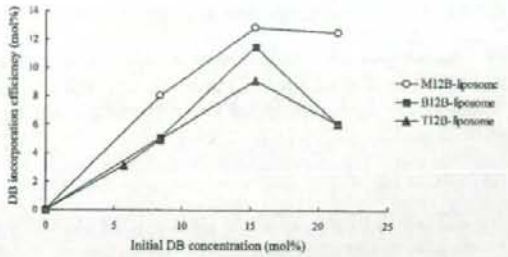

Fig. 2. Effect of Initial DB Concentration on Final DB Incorporation Levels in DB-Liposomes Composed of HSPC : Ch : OA : DB : CPT = 7 : 3 : 1 : 0—3 : 1 (Molar Ratio)

Data are average of 2 independent experiments.

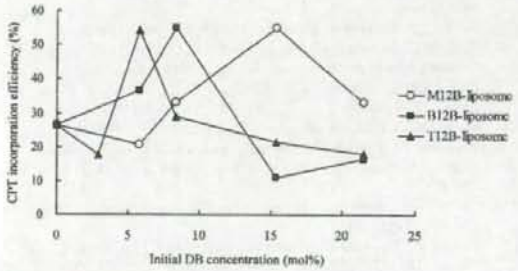

Fig. 3. Effect of Initial DB Concentration on Final CPT Incorporation Efficiency in DB-Liposomes Composed of HSPC : Ch : OA : DB : CPT = 7 : 3 : 1 : 0—3 : 1 (Molar Ratio)

Data are average of 2 independent experiments.

and 54%, respectively (Fig. 2). Also, incorporation efficiency of CPT up to 55% in all liposomes was obtained (Fig. 3). However, in the optimal formulation, DB (mol%) was different. Without DB, 26.3% of CPT was incorporated in liposomes (Control-L). The maximum CPT incorporation efficiency was obtained at the formulations of DB-liposomes: HSPC : Ch : OA : M12B : CPT = 7 : 3 : 1 : 2 : 1 (molar ratio, M12B-L), HSPC : Ch : OA : B12B : CPT = 7 : 3 : 1 : 1 : 1 (B12B-L), and HSPC : Ch : OA : T12B : CPT = 7 : 3 : 1 : 0.67 : 1 (T12B-L), as reflected about 2-fold increase (55% for M12B-L and B12B-L, and 54% for T12B-L, final drug to lipid molar ration up to 0.07) compared with Control-L. Among DB-liposomes, T12B seemed most effective to incorporate CPT in liposomes since it worked at the smallest addition amount. The excess amount of T12B decreased incorporation of CPT in liposomes, suggesting that the capacity to contain the complex of T12B with CPT might be limited in liposomes. When increase of initial CPT amount in T12B-liposomes, the incorporation efficiency of CPT was decreased (data not shown). The incorporation of DBs in liposomes seemed to decide incorporation of CPT in liposomes. Because CPT could not complex with B12B (data not shown), DBs may distribute in liposomes, and then CPT may interact with DBs and could be incorporated into the interior of the bilayers. CPT molecules may be accumulated in hydrophobic region of membranes. The presence of DB contributed increased 30% of incorporation efficiency. These findings suggested that increased CPT incorporation efficiency by DBs might be due to interaction between phenyl and dodecyloxy

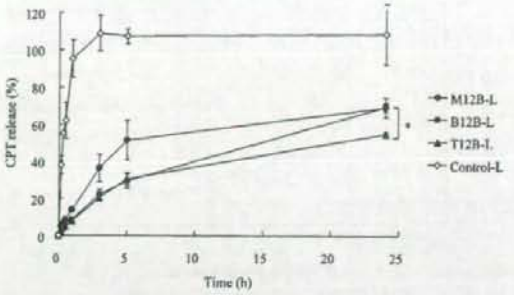

Fig. 4. Percent CPT Released as a Function of Time at 37 °C

CPT release from the liposomes of M12B-L (○), B12B-L (■), T12B-L (▲) and Control-L (◇) at the initial CPT entrapped in liposomes concentration of 200 μg/ml. CPT was monitored by membrane dialysis as described in Materials and Method using PBS as sink solution at pH=7.4. Data are expressed in the mean±standard deviation of 3 independent experiments. * $p<0.05$.

group of DBs and lactone ring of CPT over increase of acidity by carboxyl group of DBs.

***In Vitro* Drug Release** The incorporation stability of CPT in M12B-L, B12B-L and T12B-L was examined from drug release test by incubation in PBS at 37 °C, as shown in Fig. 4. The CPT released from Control-L was 100% for 3 h while that from M12B-L, B12B-L and T12B-L were 36.3, 22.3 and 20.5%, respectively. The CPT released from M12B-L was significantly higher than that from B12B-L and T12B-L for 5 h. CPT incorporated in M12B-L may be distributed at the surface of liposomes more than that in B12B-L and T12B-L, therefore CPT was released highly. During 24-h-period, M12B-L, B12B-L and T12B-L released 68.8, 69.0 and 54.5%, respectively. Release of CPT among DB-liposomes was higher T12B<B12B<M12B, and T12B-L showed significantly lower release than B12B and M12B at 24 h ($p<0.05$). This result indicated that DBs increased incorporation stability of CPT, and incorporation stability of CPT was increased with increase of the numbers of dodecyloxy-group of DBs. Dodecyloxy-group of DBs might induce drug's lactone ring to penetrate into lipid bilayers.

Fluorescence Measurements Anisotropy measurements were worthwhile as a strong indication of incorporation stability. Polarization degree of intrinsic fluorescence of CPT incorporated in the liposomes was evaluated. Figure 5 revealed that the polarization degree was CPT concentration-dependant. The polarization degree values were directly related to the kind of environment where the CPT was distributed. Free rotations in DMSO solution were related to the smallest values of polarization degree, compared to the state in liposomes, indicating that CPT molecule can move freely. M12B-, B12B- and T12B-liposomes at 0.11—0.13 μM of CPT concentration, exhibited higher polarization degree (0.47, 0.45, 0.53, respectively) compared with Control-liposomes. These results reflected that CPT molecules were inserted deeply into the lipid bilayer of liposomes. A pronounced decrease in polarization was observed below about 1 μM CPT in liposomes, revealed disordering of the lipid bilayer in the presence of CPT. Among DB-liposomes, T12B-liposome seemed to have high incorporation stability, resulting from protection of disordering property of CPT in liposomes. This result corresponded with that of release test;

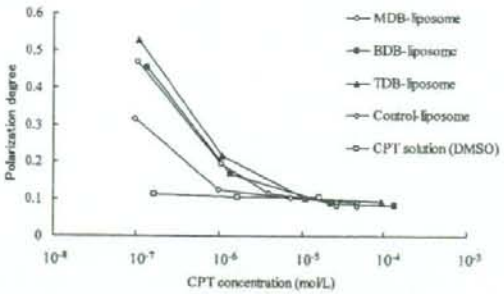

Fig. 5. Polarization Degree *versus* CPT Concentration Incorporated in M12B-Liposome (○), B12B-Liposome (■), T12B-Liposome (▲) Control-Liposome (◇) and CPT DMSO Solution at Room Temperature (24 °C)

M12B-, B12B- and T12B-liposome (HSPC : Ch : OA : M12B : CPT=7 : 3 : 1 : 1 : *x*, HSPC : Ch : OA : B12B : CPT=7 : 3 : 1 : 1 : *x* and HSPC : Ch : OA : T12B : CPT=7 : 3 : 1 : 1 : *x*, molar ratio, respectively) aqueous suspension with CPT concentration varied from 5.7×10^{-1} μg/ml to 0.1 mg/ml.

CPT in T12B-L showed the lowest release among DB-liposomes. These findings suggested that CPT in T12B-L would be incorporated into the interior of the bilayers by interaction of dodecyloxy-group of T12B with drug's lactone ring, and release slowly, while CPT in Control-L would be in contact with the water/lipid interface, be changed into the ionized form, and be released quickly.

Liposomal CPT delivery systems may be promising to cancer therapy. We have reported presently to apply this PE-Gylated formulation *in vivo* to evaluate anticancer effect.[19]

CONCLUSIONS

By incorporating various amounts of artificial lipid, DB, incorporation efficiency of CPT in liposomes increased. Additionally, we demonstrated, 4,5-tris(dodecyloxy)benzoic acid (T12B) stabilized significantly CPT in liposomes at about one third of M12B amount compared with other DBs as measured by CPT release. These findings suggested that incorporation stability of CPT in liposomes was increased, likely due to the interaction between lactone ring of CPT and dodecyloxy group more than phenyl group of DB, resulting in CPT incorporated into the interior of the bilayers.

Acknowlegements This study was supported in part by the Ministry of Education, Culture, Sports, Science and Technology of Japan, and by the Open Research Center Project.

REFERENCES

1) Wall M. E., Wani M. C., Cook C. E., Palmer K. H., Mcphail A. T., Sim G. A., *J. Am. Chem. Soc.*, **88**, 3888—3890 (1966).
2) Giovanella B. C., Stehlin J. S., Wall M. E., Wani M. C., Nicholas A. W., Liu L. F., Silber R., Potmesil M., *Science*, **246**, 1046—1048 (1989).
3) Giovanella B. C., Hinz H. R., Kozielski A. J., Stehlin J. S., Silber R., Potmesil M., *Cancer Res.*, **51**, 3052—3055 (1991).
4) Hertzberg R. P., Caranfa M. J., Hecht S. M., *Biochemistry*, **28**, 4629—4638 (1989).
5) Fassberg J., Stella V. J., *J. Pharm. Sci.*, **81**, 676—684 (1992).
6) Conover C. D., Greenwald R. B., Pendri A., Gilbert C. W., Shum K. L., *Cancer Chemother. Pharmacol.*, **42**, 407—414 (1998).
7) Fleming A. B., Haverstick K., Saltzman W. M., *Bioconjug. Chem.*, **15**, 1364—1375 (2004).
8) Mi Z., Burke T. G., *Biochemistry*, **33**, 10325—10326 (1994).
9) Warneeke A., Kratz F., *Bioconjug. Chem.*, **14**, 377—387 (2003).
10) Akimoto K., Kawai A., Ohya K., *Chem. Pharm. Bull.*, **42**, 2135—2138 (1994).
11) Daoud S. S., Fetouh M. I., Giovanella B. C., *Anticancer Drugs*, **6**, 83—93 (1995).
12) Cortesi R., Esposito E., Maietti A., Menegatti E., Nastruzzi C., *Int. J. Pharm.*, **159**, 95—103 (1997).
13) Shenderova A., Burke T. G., Schwendeman S. P., *Pharm. Res.*, **16**, 241—248 (1997).
14) Tong W., Wang L., D'souza M. J., *Drug Dev. Ind. Pharm.*, **29**, 745—756 (2003).
15) Kang J., Kumar V., Yang D., Chowdhury P. R., Hohl R. J., *Eur. J. Pharm. Sci.*, **15**, 163—170 (2002).
16) Kawano K., Watanabe M., Yamamoto T., Yokoyama M., Opanasopit P., Okano T., Maitani Y., *J. Controlled Release*, **112**, 329—332 (2006).
17) Opanasopit P., Yokoyama M., Watanabe M., Kawano K., Maitani Y., Okano T., *Pharm. Res.*, **21**, 2001—2008 (2004).
18) Watanabe M., Kawano K., Yokoyama M., Opanasopit P., Okano T., Maitani Y., *Int. J. Pharm.*, **308**, 183—189 (2006).
19) Watanabe M., Kawano K., Toma K., Hattori Y., Maitani Y., *J. Controlled Release*, in press.
20) Hara M., Takanashi Y., Tuzuki N., Kawakami H., Toma K., Higuchi A., *Cytotechnology*, **42**, 13—20 (2003).

Design of Folate-Linked Liposomal Doxorubicin to its Antitumor Effect in Mice

Atsushi Yamada,[1] Yukimi Taniguchi,[1] Kumi Kawano,[1] Takashi Honda,[2] Yoshiyuki Hattori,[1] and Yoshie Maitani[1]

Abstract

Purpose: Tumor cell targeting is a promising strategy for enhancing the therapeutic potential of chemotherapy agents. Polyethylene glycol (PEG)-coated (sterically stabilized) liposomes show enhanced accumulation on the surface of tumors, but steric hindrance by PEGylation reduces the association of the liposome-bound ligand with its receptor. To increase folate receptor (FR) targeting, we optimized the concentration and PEG spacer length of folate-PEG-lipid in liposomes.

Experimental Design: Three types of folate-linked liposomal doxorubicin were designed and prepared by optimizing the concentration and PEG spacer length of folate-PEG-lipid in PEGylated or non-PEGylated liposomes and by masking folate-linked liposomes where the folate ligand is "masked" by adjacent PEG spacers. The liposome targeting efficacy was evaluated *in vitro* and *in vivo*.

Results: In human oral carcinoma KB cells, which overexpress FR, modification with sufficiently long PEG spacer and a high concentration of folate ligand to non-PEGylated liposomes increased the FR-mediated association and cytotoxicity more than with PEGylated and masked folate-linked liposomes. On the contrary, in mice bearing murine lung carcinoma M109, modification with the folate ligand in PEGylated and masked folate-linked liposomes showed significantly higher antitumor effect than with non-PEGylated liposomes irrespective of the length of time in the circulation after intravenous injection.

Conclusions: The results of this study will be beneficial for the design and preparation of ligand-targeting carriers for cancer treatment.

A variety of targeting ligands have been examined in tumor-targeted drug carriers. Folate receptor (FR)-α is a glycosyl phosphatidylinositol-anchored membrane protein that is selectively overexpressed in >90% of ovarian carcinomas (1–3), and to various extents in other epithelial cancers, but is only minimally distributed in normal tissues (2, 4–6). FR can serve as an excellent tumor marker as well as a functional tumor-specific receptor. Folic acid, a high-affinity ligand for FR, retains its receptor-binding and endocytosis properties even if it is covalently linked to a wide variety of molecules. Therefore, liposomes conjugated to the folate ligand via a polyethylene glycol (PEG) spacer have been used to deliver chemotherapeutic agents, oligonucleotides, and markers to FR-bearing tumor cells (7–16). The targeting efficiency of folate-linked vesicles was affected by the amount of folate-PEG-lipid. It was reported that a higher molar fraction of folate-PEG-lipid in folate-linked liposomes reduced liposome uptake into cells (17). Folate molecules can form dimers, trimers, and even self-assembling tubular quartets at higher concentrations (18). Because FR can only bind one molecule of folic acid (19), such self-assembled multimers of folic acid are incapable of binding to FR.

PEGylated liposomes, called sterically stabilized liposomes, evade uptake by the reticuloendothelial system and show enhanced accumulation in tumors as a result of an enhanced permeability and retention effect. Liposomes were modified with folate to further increase targeting to FR and drug uptake by tumors. However, when targeting moieties are employed, circulation times are often decreased *in vivo* due to recognition by the reticuloendothelial system (9). As a result, the advantage of increased drug retention on the tumor surface by PEGylation is obscured by accelerated clearance of folate-linked formulations. Furthermore, steric hindrance by PEGylation reduces the association of the liposome-bound ligand with its receptor (8). Therefore, the density and PEG spacer length of the targeting ligand and PEGylation of liposomes are known to be critical characteristics for ligand-receptor interaction. However, there have been few studies concerned with the optimization of these factors.

In our previous studies, we have reported on the optimal folate concentration and PEG spacer length with nanoemulsions and polymer micelles (20, 21). However, in these cases,

Authors' Affiliations: [1]Institute of Medicinal Chemistry, Hoshi University, Tokyo, Japan and [2]Fukushima Medical University School of Nursing, Fukushima-City, Japan

Received 1/21/08; revised 5/16/08; accepted 6/6/08.

Grant support: Ministry of Education, Culture, Sports, Science and Technology, Japan, Ministry of Health, Labor and Welfare, Japan, and Open Research Center Project.

The costs of publication of this article were defrayed in part by the payment of page charges. This article must therefore be hereby marked *advertisement* in accordance with 18 U.S.C. Section 1734 solely to indicate this fact.

Note: Supplementary data for this article are available at Clinical Cancer Research Online (http://clincancerres.aacrjournals.org/).

Requests for reprints: Yoshie Maitani, Institute of Medicinal Chemistry, Hoshi University, Shinagawa, Ebara 2-4-41, Tokyo, 142-8501 Japan. Phone: 81-3-5498-5048; Fax: 81-3-5498-5048. E-mail: yoshie@hoshi.ac.jp.

doi:10.1158/1078-0432.CCR-08-0159

Translational Relevance

PEGylated liposomes show enhanced accumulation on the surface of tumors by long circulation. FR is selectively overexpressed to various extents in epithelial cancers. Folic acid is a high-affinity ligand for FR. The targeting efficiency of folate-linked vesicles was affected by the amount of both folate-PEG-lipid and PEG-lipid. To increase FR targeting, we optimized the concentration and PEG spacer length of folate-PEG-lipid in liposomes. In mice bearing murine lung carcinoma M109, modification with the folate ligand in PEGylated and masked folate-linked liposomes where the folate ligand is "masked" by adjacent PEG spacers showed significantly higher antitumor effect than with non-PEGylated liposomes after intravenous injection. This finding suggested that tumor targeting was achieved by less PEGylated carriers with ligand. Three anthracycline liposomal preparations including PEGylated liposomal doxorubicin (Doxil) are currently on the market, and many other liposomal formulations of antineoplastic drugs are in preclinical or clinical trials. Therefore, this strategy will be applied to such drug formulations for future practice of cancer medicine. The results of this study will be beneficial for the design and preparation of ligand-targeting carriers to deliver chemotherapeutic agents and gene for cancer treatment and contrast agents for the detection of solid tumors.

PEG-lipid and PEG polymer are the main components that form the nanoemulsions and polymer micelles, respectively, so we could not evaluate effect of folate-PEG-lipid alone on targeting to tumors. Because liposomes can be prepared without PEG-lipid, we can estimate the optimal density and PEG spacer length of folate-PEG-lipid for FR targeting to produce a balance between longer circulation time and FR targeting.

Here, we designed and prepared various folate-linked liposomes to increase the level of FR-targeting. In this study, we evaluated folate-mediated association of liposomal doxorubicin with human oral carcinoma KB cells and murine lung carcinoma M109 cells, which both overexpresses FR, in terms of the effect of PEG spacer length and the ratio of modification of the folate ligand of liposomes with or without PEG-coating and of the degree of masking of folate ligands on liposomes by adjacent PEG. Furthermore, the antitumor effect of these liposome preparations was investigated *in vitro* and *in vivo*.

Materials and Methods

Materials. Hydrogenated soybean phosphatidylcholine (HSPC) was obtained and amino-PEG-distearylphosphatidylethanolamine (amino-PEG-DSPE; PEG mean molecular weights, 2,000, 3,400, and 5,000) and methoxy-PEG-distearylphosphatidylethanolamine (mPEG-DSPE; PEG mean molecular weights, 2,000 and 5,000) were kind gifts from the NOF. Cholesterol, doxorubicin hydrochloride, and high-performance liquid chromatography-grade acetonitrile were purchased from Wako Pure Chemical Industries. Folate-PEG-DSPEs (F-PEG_{2000}-DSPE, F-PEG_{3400}-DSPE, and F-PEG_{5000}-DSPE), which are conjugates of folic acid and amino-PEG-DSPE, were synthesized as reported previously (8, 20). Folate-deficient RPMI 1640 and fetal bovine serum were obtained from Invitrogen. Other reagents used in this study were of reagent grade.

Preparation of folate-linked liposomal doxorubicin. Liposomes were prepared from hydrogenated soybean phosphatidylcholine/cholesterol = 55/45 (mol/mol) by a dry-film method. Briefly, all lipids were dissolved in chloroform, which was removed by evaporation. The thin film was hydrated with citrate buffer (300 mmol/L adjusted to pH 4.0 with NaOH) at 60°C by vortex mixing and sonication. Targeted formulations were prepared by mixing nontargeted liposomes with micelles of mPEG-DSPE and/or F-PEG-DSPE to allow incorporation of targeting ligands at 60°C for 1 h by the postinsertion technique (22). The number of targeting ligands was controlled by altering the concentration of micelles added to the liposomes before loading with doxorubicin.

Schematic diagrams (Fig. 1) show three kinds of folate-PEG-liposomes: overhanging folate outside non-PEGylated liposomes (NL), PEGylated liposomes with a $mPEG_{2000}$ layer (SL), and masked folate inside a $mPEG_{5000}$ layer of liposomes (ML). NLs with folate ligands were prepared by incubation of NL with an aqueous dispersion of F-PEG-DSPE (from 0.01 to 0.5 mol% total lipids; Fig. 1A). SLs modified with folate were prepared by incubation of NLs with a total of 2.5 mol% PEG-lipids of $mPEG_{2000}$-DSPE and varying percentages of F-PEG_{5000}-DSPE (F5; Fig. 1B). MLs were prepared by incubation of NLs with an aqueous dispersion of 0.25 mol% F-PEG_{2000}-DSPE and 0.75 mol% $mPEG_{5000}$-DSPE (Fig. 1C). NLs linked with F-PEG_{2000}-DSPE, F-PEG_{3400}-DSPE, or F-PEG_{5000}-DSPE are henceforth abbreviated as F2-NL, F3-NL, and F5-NL, respectively, and SL linked with F-PEG_{5000}-DSPE is abbreviated as F5-SL. The number before the abbreviated term of F5-NL in some descriptions indicates the mol% F-PEG-DSPE of total lipids. For instance, 0.25F5-NL indicates liposomes with 0.25 mol% F-PEG_{5000}-DSPE of total lipids, and 0.25F5-SL indicates liposomes with total 2.5 mol% PEG-lipids composed of 2.25 mol% $mPEG_{2000}$-DSPE for steric stabilization and 0.25 mol% F-PEG_{5000}-DSPE. The resulting mean diameter and ζ potential of liposomes were determined by dynamic light scattering and electrophoresis methods, respectively (ELS-800; Otsuka Electronics) at 25°C after diluting the liposome suspension with water.

Next, these liposomes were actively loaded with doxorubicin by a pH gradient method (23). After the external pH was adjusted to pH 7.4, liposomes were incubated with doxorubicin [drug/lipid = 1:5 (w/w)] at 60°C for 25 min. Doxorubicin loading efficiency was determined by separating unencapsulated from encapsulated drug on a Sephadex G-50 column. Doxorubicin concentration was determined by measuring absorbance at 480 nm (UV-1700 Phamaspec; Shimadzu). The final liposomal doxorubicin was suspended in 150 mmol/L NaCl. The final total lipid concentration of folate-linked liposomes was 18.6 mg/mL.

In vitro drug release of liposomes. *In vitro* release of doxorubicin from the liposomal formulation was analyzed by membrane dialysis against PBS (pH 7.4) at 37°C under sink condition. Briefly, 1 mL liposomal doxorubicin (0.2 mg/mL doxorubicin) was placed in a dialysis tube (seamless cellulose tube membranes; Viskase Sales) with a molecular weight cutoff of 12,000 to 14,000 and then suspended in a temperature-controlled, jacketed flask containing 100 mL PBS. After various time intervals, aliquots of the medium were withdrawn. The doxorubicin concentration was analyzed using a fluorophotometer (Wallac 1420 ARVOsx multilabel counter; Perkin-Elmer Life Science) with excitation and emission wavelengths of 485 and 535 nm, respectively.

Cell culture. KB cells were obtained from the Cell Resource Center for Biomedical Research, Tohoku University. The human lung adenocarcinoma A549 cell line [FR(-)] was kindly provided by OncoTherapy Science. The cells were cultured in folate-deficient RPMI 1640 with 10% heat-inactivated fetal bovine serum and 50 μg/mL kanamycin sulfate in a humidified atmosphere containing 5% CO_2 at 37°C. The cells were prepared by plating 3×10^5 per well in a 12-well culture plate for flow cytometry analysis or 1×10^4 per well in a 96-well culture plate for cytotoxicity analysis for 1 day before the assay.

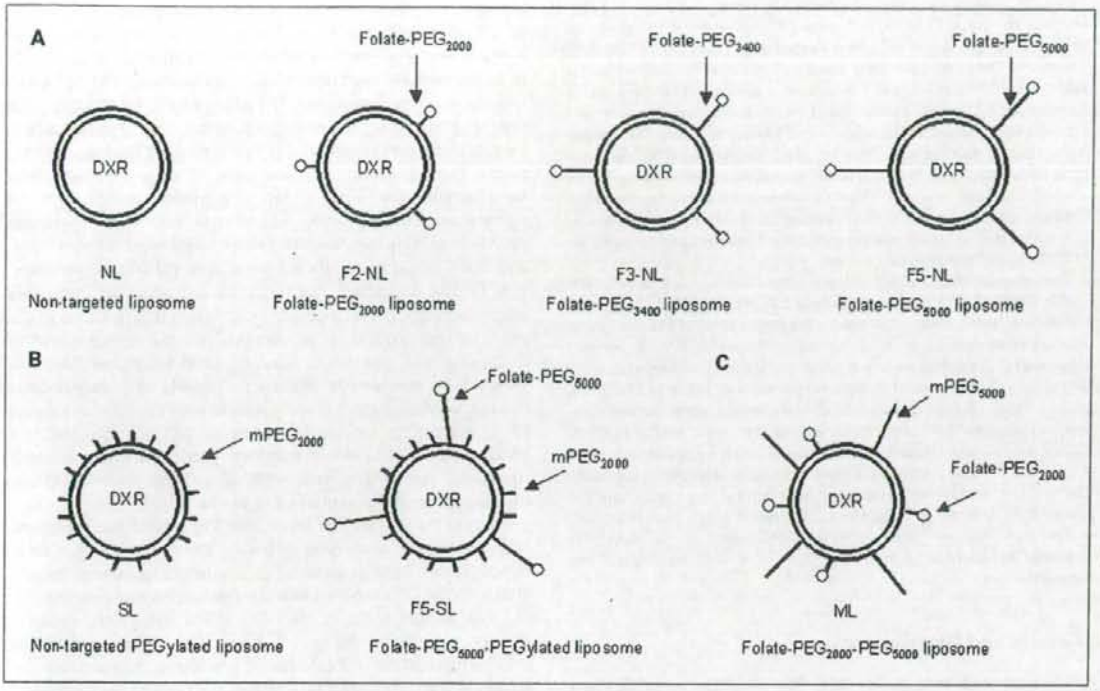

Fig. 1. Schematic diagrams of folate-linked liposomal doxorubicin (*DXR*).

Murine lung carcinoma M109 cells (high FR-expressing cell line) were obtained from Division Chemotherapy (Translational Research Center), Chiba Cancer Center. M109 cells were used to evaluate the accumulation of folate-linked liposomes in tumor tissue and therapeutic effect. The cells were subcultured by employing the biogenic system of BALB/c mice.

Cellular uptake of liposomal doxorubicin assessed by flow cytometry. KB and A549 cells were incubated with liposomal doxorubicin containing 20 μg/mL doxorubicin diluted in 1 mL medium for 1 h at 37°C. In free folate competition studies, 1 mmol/L folic acid was added to the medium. After incubation, the cells were washed with cold PBS (pH 7.4) three times, detached with 0.02% EDTA-PBS for KB cells and with 0.05% trypsin for A549 cells, and then suspended in PBS containing 0.1% bovine serum albumin and 1 mmol/L EDTA. The suspended cells were directly introduced into a FACSCalibur flow cytometer (Becton Dickinson) equipped with a 488 nm argon ion laser. Data for 10,000 fluorescent events were obtained by recording forward scatter, side scatter, and 585/42 nm fluorescence. The autofluorescence of cells incubated with medium without drugs for 1 h was taken as a control.

Confocal laser scanning microscopy. After incubation with liposomes containing 20 μg/mL doxorubicin for 1 h, the medium was removed, and the cells were washed three times with PBS and fixed with 10% formaldehyde PBS at 37°C for 20 min. Then, the cells were coated with Aqua Poly/Mount (Polyscience) to prevent fading and covered with coverslips. The fixed cells were observed with a Radiance 2100 confocal laser scanning microscope (Bio-Rad).

In vitro *cytotoxicity study.* KB cells were incubated with liposomal doxorubicin containing 0.02 to 100 μg/mL doxorubicin diluted in 100 μL medium for 2 h at 37°C. After incubation, the cells were washed with cold PBS (pH 7.4) and cultured in fresh medium for 48 h. Then, 10 μL WST-8 (Dojindo Laboratories) stock solution (5 mmol/L) was added to each well, and the plate was incubated for 1 h at 37°C. Cell viability was assessed by measuring the absorbance at 450 nm.

Pharmacokinetic analysis. Male ddY mice (body weight, ~28 g) were obtained from Tokyo Laboratory Animal Science. Liposomes were injected as a single intravenous bolus via the lateral tail vein at a dose of 5 mg/kg doxorubicin. At 3, 6, and 24 h after the injection, blood was collected and centrifuged to obtain serum. Serum doxorubicin levels were determined by a high-performance liquid chromatography method (24). The high-performance liquid chromatography system was composed of a LC-10AS pump (Shimadzu), a SIL-10A autoinjector (Shimadzu), a RF-10A_{XL} fluorescence detector (excision, 482 nm; emission, 550 nm; Shimadzu), and a YMC-Pack ODS-A, 150 × 4.6 mm i.d. column (YMC). The mobile phase was 0.1 mol/L ammonium formate (pH 4.0)/acetonitrile [7:3 (v/v)] with a flow rate of 1.0 mL/min. The concentration of doxorubicin in each sample was determined using a calibration curve, with daunomycin as the internal standard. Pharmacokinetic variables were calculated using a bootstrap method, including area under the concentration curve (from 3 to 24 h; AUC) and clearance (25).

Microscopic imaging of tumor section. M109 cells were inoculated subcutaneously into female CDF_1 mice (5 weeks old; Sankyo Lab Service). When the tumor volume reached ~100 mm^3, each preparation of liposomes, SL, 0.25F5-SL, ML, and free doxorubicin, was injected intravenously at 5 mg/kg doxorubicin body weight. Twenty-four hours after liposome injection, the mice were sacrificed, and tumor tissues were collected and immediately frozen in dry ice. The tumors were embedded in OCT compound (Tissue-Tek; Sakura Finetechnical) and processed by frozen sectioning at 10 μm. Each frozen section was mounted on a MAS-coated slide glass (SUPER-FROST; Matsunami). The specimens were fixed in 4% paraformaldehyde for 15 min at room temperature and washed three times with

PBS-0.02% Tween 20. Protein blocking was done for 30 min at room temperature using PBS-0.02% Tween 20 containing 0.3% skimmed milk, and the specimens were then washed three times with PBS-0.02% Tween 20. The specimens were incubated with biotin-conjugated rat anti-mouse CD31 (PECAM-1) monoclonal antibody (BD Biosciences Pharmingen), diluted 1:200, for 1 h at room temperature and subsequently washed three times with PBS-0.02% Tween 20. Immunofluorescent staining was done by using streptavidin-FITC (Invitrogen), diluted to 1:200, for 1 h at room temperature. The specimens were washed for a final time with PBS-0.02% Tween 20, and coverslips were mounted on the glass slides with prolong Antifade (Aqua Poly/Mount; Polysciences). The specimens were examined microscopically using an ECLIPSE TS100 microscope (Nikon).

Therapeutic studies. M109 cells were inoculated subcutaneously into female CDF_1 mice (5 weeks old; Sankyo Lab Service). When the tumor volume reached ~100 to 200 mm^3, each preparation of liposomes was injected intravenously at 8 or 10 mg/kg doxorubicin body weight. Liposomal doxorubicin or free doxorubicin solution was injected via a lateral tail vein. The control group was injected with saline (0.1 mL/10 g body weight). Tumor volumes and body weight were measured at regular intervals. The tumor size was measured with vernier calipers. Tumor volume was calculated using the following equation: volume = $\pi / 6 \times LW^2$, where L is the long diameter and W is the short diameter. The animal experiments were done with ethical approval from the Institutional Animal Care and Use Committee at Hoshi University.

Statistical analysis. The statistical significance of the data was evaluated by analysis of Student's t test. $P \leq 0.05$ was considered significant.

Results and Discussion

We supposed that active targeting by folate modification could be achieved based on success in passive targeting of drug carriers by PEGylation. To optimize folate presentation, the design of folate-linked liposomes used in this study is presented in Fig. 1. We prepared three kinds of folate-linked liposomes: overhanging folate-linked NL and SL and masking folate-linked ML. For overhanging folate-linked liposomes, we used various concentrations and PEG spacer lengths of F-PEG-DSPE to attain high-affinity binding. Accordingly, liposomal formulations were characterized for their *in vitro* efficacy of drug delivery and for their *in vivo* pharmacokinetics and tumor therapeutic efficacy. Optimal formulation of folate-linked liposomes was achieved by optimizing the folate ligand density and PEG spacer length on the surface of the liposomes.

Preparation of folate-linked liposomal doxorubicin. For efficient drug delivery to the target site, drugs should be stably entrapped in liposomes. In this study, the sequence of processes of folate modification on the liposome and doxorubicin loading was examined to efficiently encapsulate doxorubicin in liposomes. We used three kinds of procedures: (A), (*a*) folate modification on liposomes, (*b*) pH gradient by changing the outside pH, and (*c*) doxorubicin loading; (B), (*a*) pH gradient by changing the outside pH, (*b*) doxorubicin loading, and (*c*) folate modification on liposomes; (C), (*a*) pH gradient by changing the outside pH, (*b*) folate modification on liposomes, and (*c*) doxorubicin loading. The liposomes prepared using procedures (A) to (C) exhibited 95%, 15.6%, and 7.3% entrapment efficiencies of doxorubicin, respectively. This finding suggested that folate modification on liposomes affected the liposomal membrane, resulting in a decrease in the pH gradient and then a decrease in the entrapment of doxorubicin. Doxorubicin loading after folate modification gave a high entrapment efficiency of >95% at a drug-to-total lipid ratio of 1:5 (w/w), corresponding with the previous report (26). Hereafter, we used procedure (A) for doxorubicin entrapment. In all cases, the average particle diameter of each liposome was ~100 nm with a narrow, monodisperse distribution and ζ potential of -9 to -14 mV.

Effect of F-PEG-DSPE in folate-linked liposomal doxorubicin on cellular uptake and drug release. First of all, the time dependency of the amount of folate-linked liposomes associated with the cells was evaluated by fluorescence of doxorubicin in cells (Supplementary Fig. S1). Flow cytometry analysis showed a shift in the curve, indicating a clear increase in cellular association of folate-linked liposomes after incubation. Until the second hour of incubation, the cellular association of folate in F5-NL increased with the increasing amount of folate more than NL. The associated amount of doxorubicin in F5-NL reached a plateau after 2 to 3 h. Because folate-linked liposomes rapidly associate with FR overexpressed KB cells, it was clarified that typical saturation was achieved within the second hour of incubation (27). Thereafter, incubation for 1 h was used in the following experiments.

Next, we examined the optimal concentration and PEG spacer length of F-PEG-DSPE in liposomes for cellular uptake. For the influence of the PEG spacer length to uptake, a larger PEG spacer, F-PEG_{5000}-DSPE, showed higher association after a 1 h incubation (Fig. 2A). With regard to the density of F-PEG-DSPE, the highest level of folate modification (0.5 mol%) showed the highest uptake regardless of PEG spacer length except for F5-NL. F5-NL with 0.25 mol%

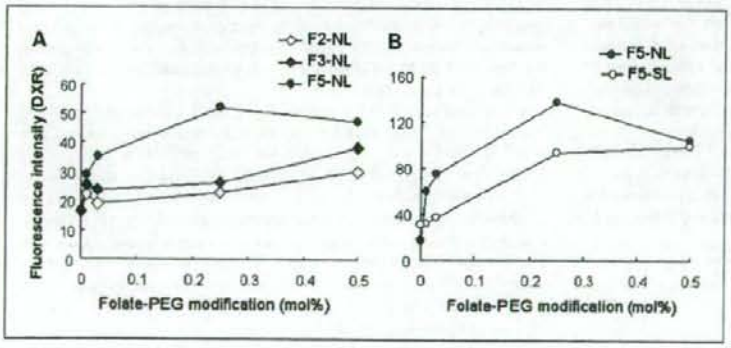

Fig. 2. Dependency of cellular association of non-PEGylated (*A*) and PEGylated (*B*) liposomal doxorubicin on folate-PEG concentration. Cell-associated doxorubicin was determined by flow cytometry analysis after KB cells were incubated with 20 μg/mL doxorubicin for 1 h at 37°C. Each analysis was generated by counting 10^4 cells.